

1 **Persistent effect of El Niño on global economic growth**

2 Christopher W. Callahan^{1,2*} & Justin S. Mankin^{1,2,3,4}

3
4 ¹Program in Ecology, Evolution, Environment and Society, Dartmouth College, Hanover, NH

5 ²Department of Geography, Dartmouth College, Hanover, NH

6 ³Department of Earth Sciences, Dartmouth College, Hanover, NH

7 ⁴Ocean and Climate Physics, Lamont-Doherty Earth Observatory of Columbia University, Palisades, NY

8 *Corresponding author, Christopher.W.Callahan.GR@dartmouth.edu

9
10 *This article has now been published in Science. The final article is available at the “Peer-reviewed*

11 *Publication DOI” link on the right-hand-side of this webpage or at this link:*

12 <https://www.science.org/doi/10.1126/science.adf2983>. Please feel free to contact the corresponding

13 *author with questions or comments.*

14
15 **El Niño-Southern Oscillation (ENSO) shapes extreme weather globally, causing myriad**

16 **socioeconomic impacts, but whether economies recover from ENSO events and how anthropogenic**

17 **changes to ENSO will affect the global economy are unknown. Here we show that El Niño**

18 **persistently reduces country-level economic growth, attributing \$4.1T and \$5.7T in global income**

19 **losses to the 1982-83 and 1997-98 events, respectively. Increased ENSO amplitude and**

20 **teleconnections from warming cause \$84T in 21st-century economic losses in an emissions scenario**

21 **consistent with current mitigation pledges, but these effects are shaped by stochastic variation in**

22 **the sequence of El Niño and La Niña events. Our results highlight the sensitivity of the economy to**

23 **climate variability independent of warming and the potential for future losses due to anthropogenic**

24 **intensification of such variability.**

25 As the leading mode of interannual climate variability, El Niño-Southern Oscillation (ENSO)

26 integrates a wide range of Earth system processes (1). El Niño events shift deep convection from the

27 western to the eastern Pacific, shaping global weather through “teleconnections” (2, 3). The resulting

28 temperature and hydroclimate extremes have many well-documented impacts, including flooding (4, 5),

29 crop losses (6, 7), and civil conflict (8). Many climate models project that warming will increase El Niño

30 amplitude (9, 10) and frequency (11), with potentially devastating socioeconomic impacts (12).

31 Despite ENSO’s global impacts, however, empirical climate-economy studies have generally

32 focused on temperature and rainfall averages (13–16) or variability (17), leaving the costs of changes in

33 modes of climate variability unquantified. While studies have shown that El Niño reduces

34 contemporaneous economic growth (18–20) and drives commodity price fluctuations (21–23), it remains

35 unclear if and for how long its impacts persist. Distinguishing between transient and persistent impacts on
36 economic growth is essential. Transient impacts (“level effects”) are quickly recovered, as an economy
37 rebounds to its original trajectory. Persistent impacts (“growth effects”) reduce an economy’s ability to
38 grow, compounding exponentially in time. Poor observational constraints on growth effects limit our
39 understanding of the economic costs of ENSO and climate damages broadly (24–26).

40 Here we estimate the effect of ENSO on past and future economic growth, accounting for the
41 spatiotemporal heterogeneity of ENSO teleconnections. We define ENSO by the E-index and C-index
42 (27) (Fig. S1). These metrics of El Niño and La Niña, respectively, capture the nonlinear feedbacks that
43 drive ENSO (Methods). We define country-level teleconnections for each index (τ^E and τ^C) using
44 correlations between the indices and country-level temperature and rainfall (Methods, Fig. S2).
45 Teleconnections are strongest in tropical countries and weaker in the midlatitudes (Fig. 1a), consistent
46 with the physical responses of regional climate to tropical variability (28).

47 We use a distributed lag regression model to quantify the effect of ENSO on growth in national
48 Gross Domestic Product per capita (GDPpc) from 1960-2019. Departing from previous work (8, 19, 20),
49 we interact the E- and C-indices with teleconnections to allow the economic effect of ENSO to vary
50 smoothly as a function of teleconnection strength (29) (Methods). Our model compares economic growth
51 before and after El Niño events to assess their cumulative effects over time and distinguish growth from
52 level effects (Methods). We focus on the five years following El Niño events, but also evaluate effects for
53 more than ten years as well as for La Niña. We then couple these empirical estimates with climate model
54 projections to assess the future economic effects of changes to ENSO amplitude and teleconnections.

55

56 **El Niño persistently reduces economic growth**

57 El Niño events persistently decrease economic growth (Fig. 1b). The magnitude of this effect is
58 determined by the strength of each country’s E-index teleconnection. In Peru ($\tau^E = 1.18$), for example, a
59 1-standard-deviation (s.d.) El Niño event decreases growth by 1.3 percentage points (p.p.) in the year of
60 the event (95% confidence interval [CI]: 0.9 – 1.7 p.p.). After five years, growth in Peru has declined by
61 6.2 p.p. (CI: 4.7 – 8.2) (Fig. 1b). By contrast, weakly teleconnected countries experience small and
62 uncertain effects (Fig. 1b). Interacting El Niño and teleconnections allows us to calculate marginal effects
63 for each country based on their τ^E value (Fig. 1c) and allows statistical significance to be determined by
64 uncertainty in the distributed lag model (Fig. 1c hatching), rather than prescribing “teleconnected” and
65 “non-teleconnected” countries. 56% of countries experience significant declines in growth 5 years after El
66 Niños, averaging 2.3 p.p., not simply level effects from which they recover immediately (Fig. 1d).

67 These negative effects are robust to using alternative ENSO indices, growth data, standard error
68 clustering, or teleconnection metrics, as well as excluding the most strongly teleconnected countries (SM

69 Text, Figs. S3-S5). They also vary little over the 1960-2019 period, indicating little effect heterogeneity
70 in time (Fig. S6). ENSO indices vary through time but not space, raising the possibility that our results are
71 confounded by time-varying global economic shocks. However, alternative specifications demonstrate
72 that time-varying confounders are not driving our results: Adding country-specific trends to control for
73 technological or demographic changes has little effect (Fig. S4) since ENSO is stochastic (30) and
74 measured by detrended indices. Using a spatially varying country-level index of ENSO or discretizing the
75 sample into teleconnected and non-teleconnected groups allow us to include both country and year fixed
76 effects, and yield results as strong as our main estimates (Methods, Fig. S7), but we do not use these
77 models in our main analysis since they do not preserve the independent and joint effects of ENSO
78 amplitude and teleconnections (Methods). Bootstrap resampling by year or dropping each year or country,
79 ensuring that single years or countries are not driving the results, yield similar effects (Fig. S3). Finally,
80 dropping the 1983 and 1998 El Niño events, which coincided with financial crises, reduces the magnitude
81 of ENSO effects by only ~12% (Fig. S4).

82 Our main observational analysis (Figs. 1, 2) uses 5 lags, which reflects a balance between tracing
83 the long-run response to ENSO and a concern for statistical power given the short observational record.
84 Additional lags fit the data better, but at the cost of model stability; using 5 lags balances these effects
85 (Fig. S8). Yet models with more lags reveals that El Niño effects can persist to 12 years or beyond,
86 though a rebound begins after ~10 years (Figs. S8, S9), implying that our 5-year results for the historical
87 costs of El Niño are conservative. After >14 years, the effects of ENSO cannot confidently be
88 distinguished from zero. However, data simulations using a perfect model framework, where we impute a
89 permanent effect of El Niño to data, demonstrate that models with many lags can yield insignificant
90 coefficients due to the reduced sample size and large number of parameters (Methods, Fig. S8). The
91 perfect model framework implies that, even if the real-world effects of ENSO were permanent, we may
92 not be able to detect them given the short observational record. Finally, even if economies do eventually
93 rebound from ENSO, the fact that damages accumulate for more than a decade means that the costs of
94 climate variability are much larger than typically assumed in climate-economy models (31).

95 Our empirical model includes both the E-index and C-index, allowing us to distinguish the effects
96 of eastern Pacific (EP) El Niño and central Pacific (CP) La Niña (Methods). CP La Niña events have
97 beneficial effects (Fig. S10), but they are several times weaker than the negative effects of EP El Niño
98 and statistically insignificant under alternative standard error clustering (Table S2). These results reflect
99 the skewness of ENSO itself, whereby EP El Niños tend to be stronger than both La Niñas and CP El
100 Niños, and are consistent with studies showing that La Niña's economic effect is small (19, 20).

101 The countries most affected by ENSO are generally lower-income, tropical countries (19).
102 However, high-income countries also experience significant negative effects (Fig. S4), consistent with

103 work showing that these countries are impacted by extreme rainfall (32) and heat (33), both of which
104 ENSO affects. We also identify persistent losses across countries that experience wetting and drying in
105 response to El Niño (Fig. S4), as both anomalously low and high rainfall can be damaging (32). We
106 emphasize that some regions may experience benefits from El Niño or losses from La Niña. Our goal is to
107 estimate a globally generalizable response to ENSO. That our findings are robust across multiple lines of
108 country heterogeneity provides confidence that they are generalizable, even if individual regions may
109 respond differently.

110

111 **Losses from historical El Niño events**

112 The persistent effect of ENSO implies that historical El Niño events have altered the income
113 growth of teleconnected countries, potentially generating large economic losses. Here we quantify the
114 costs of the two largest El Niño events in the last 60 years, in 1982-83 and 1997-98 (Fig. 2). Because an
115 El Niño can trigger a subsequent La Niña (34), our analysis incorporates both the negative effects of each
116 El Niño and the benefits of the following La Niña (Methods). Furthermore, because these events
117 coincided with unrelated currency crises, we use a model excluding these events to more conservatively
118 calculate their impacts (Fig. S4).

119 Consider strongly teleconnected Peru ($\tau^E = 1.18$): Its GDPpc declined in 1998 and stagnated for
120 three more years (Fig. 2a). Given the 1997 financial crisis, Peru's slower growth in 1998 is not entirely
121 attributable to ENSO, but Peru's economy would have grown more quickly if the 1997-98 El Niño had
122 not occurred (Methods). Income for the average Peruvian would have been some \$1,246 greater five
123 years later in 2003 absent the event (CI: \$853 – \$1,793), a 19% increase (Fig. 2a). Other tropical countries
124 such as Ecuador, Brazil, and Indonesia lost anywhere from 5% to 19% of GDPpc (Fig. S11).

125 We estimate global losses from the 1982-83 and 1997-98 events to be trillions of dollars each
126 (Fig. 2b, S11). Our estimates exceed previous ones because we account for ENSO's growth effects: one
127 study placed the total costs of the 1997-98 El Niño at \$36 billion (35). Our accounting has losses from the
128 1997-98 event rising to three orders of magnitude more than that estimate, some \$5.7T by 2003 (CI:
129 \$2.3T – \$9.2T). The earlier 1982-83 event tallied \$4.1T by 1988 (CI: \$2.3T – \$6T). The greater costs of
130 the 1997-98 event result both because it was a stronger El Niño and because the global economy was
131 larger. Absent the compensating benefits of the subsequent La Niñas, the 1983 (1998) event would have
132 produced losses of \$4.4T (\$8T) (Fig. 2b).

133 We focus on 5 lags in this historical analysis to balance the imperatives of tracking the effects of
134 ENSO and maximizing statistical power (Fig. S8). Because the effect of El Niño appears to persist for
135 more than five years (Fig. S8), the ultimate toll of these events may be even higher than we show here. In
136 fact, by incorporating growth reductions following the event and including all countries in a single

137 framework, we show that estimates focusing on physical asset losses in low-income countries have
138 strongly underestimated the global economic toll of El Niño.

139

140 **Climate model projections of ENSO**

141 ENSO's persistent effect raises the question of how it will shape the global economy with further
142 warming. Using climate model simulations from the sixth phase of the Coupled Model Intercomparison
143 Project (CMIP6) that skillfully simulate eastern Pacific SSTs, we analyze projected changes to ENSO
144 under four Shared Socioeconomic Pathways (SSPs) (Methods).

145 El Niño amplitude and teleconnections both increase with warming in CMIP6 (Fig. 3). This
146 response is not scenario-dependent, likely due to the influence of internal climate variability on forced
147 ENSO changes (36–38). Median amplitude increases by 5 – 21% across scenarios (Fig. 3a), a function of
148 stronger wind-ocean coupling in the eastern Pacific (9, 12). Global mean teleconnections increase by 4 –
149 15% (Fig. 3b), consistent with a more energetic atmospheric response to El Niño (39, 40). Despite these
150 forced responses, internal variability (proxied by multiple realizations from each model) can vary these
151 responses by >60 p.p. (Fig. 3a, b, lower lines).

152 Beyond amplitude and teleconnection changes, climate projections differ in their E-index time
153 series. Due to ENSO's sensitivity to initial conditions (36–38) and multidecadal variability (41, 42), a
154 wide range of E-index values across models and scenarios can occur in a given year, even controlling for
155 amplitude (Fig. 3c, S12). For example, Figure 3c shows two SSP2-4.5 simulations with similar amplitude
156 changes and E-index skewness but different sequences of EP El Niños and La Niñas. As quantified by the
157 sum of the E-index over the 21st century, MIROC-ES2L r6i1p1f2 experiences strong El Niño events while
158 CESM2-WACCM r3i1p1f1 is dominated by La Niña events. Such differences in the ENSO sequence
159 shape projected damages, as an El Niño-dominated time series yields greater damages than a La Niña-
160 dominated one due to their differential effects (Fig. S10). Crucially, because El Niños are stronger than
161 La Niñas, the expectation from increased ENSO amplitude is net losses.

162 We combine these projections with our empirical estimates to quantify the economic effects of
163 changes in ENSO. We use the SSPs as baselines against which we calculate country-level growth changes
164 based on ENSO amplitude and teleconnection projections (Methods). Departing from our historical
165 estimates (Figs. 1 and 2), we project future ENSO damages with a model that extends damages out to ~14
166 years because we can confidently detect damage accumulation that long, yet cannot identify truly
167 permanent growth effects due to the short observational record (Fig. S8). As such, we make the
168 conservative choice to allow economies to fully recover from future ENSO events after 14 years in our
169 projections (Methods). This simplifying choice assumes that the time persistence of ENSO impacts is
170 homogenous. However, it is possible that different countries recover over different time scales. For

171 example, weakly teleconnected countries may rebound more quickly (Fig. 1d), and the sectoral makeup of
172 an economy (e.g., agriculture- vs. manufacturing-dependent) may affect the speed with which it can
173 reinvest in new growth after El Niño events. Further research into whether, how, and over what time
174 scales economies recover from El Niño events would reduce uncertainty in our projections and help
175 economies manage extreme climate events more broadly.

176

177 **Economic impacts of future ENSO changes**

178 Projected anthropogenic changes to El Niño amplitude and teleconnections will likely cause
179 substantial economic losses over the 21st century (Fig. 4). Under a 2% discount rate (43) and a
180 socioeconomic scenario consistent with current pledges to reduce greenhouse gas emissions (44) (SSP2-
181 4.5), the median cumulative 2020-2099 global losses are \$84T (Fig. 4a), a ~1% reduction in global
182 economic output over the 21st century. In all four scenarios, median losses exceed \$18T and damages are
183 negatively skewed, consistent with the asymmetry in ENSO itself.

184 The range of these projections is large. Under SSP2-4.5, the 95% range spans losses of \$453T to
185 benefits of \$80T (we write this CI as -\$453T – +\$80T) across 86,000 combinations of 86 simulations and
186 1,000 regression bootstraps (Fig. 4a). Reducing the discount rate to 1% amplifies median losses under
187 SSP2-4.5 to \$130T (-\$687T – +\$130T), while increasing it to 5% diminishes losses to \$26T (-\$162T –
188 +\$34T). The extreme end of these ranges implies a ~5% reduction in global economic output. In highly
189 teleconnected countries, ENSO changes cause GDPpc reductions of >1% per year, though uncertainty is
190 high even in these countries (Fig. S11).

191 Despite this range across realizations, models, and scenarios, increases in ENSO amplitude and
192 teleconnections are systematically related to greater economic losses (Fig. 4b, c). Each 1% increase in
193 ENSO amplitude is associated with \$4.1T in additional discounted losses over the 21st century ($p <$
194 0.001), and each 1% increase in teleconnections is associated with \$6.3T in losses ($p <$ 0.001). These
195 findings build upon previous projections of changes in ENSO amplitude (9, 11) and teleconnections (39,
196 40), demonstrating global socioeconomic effects of these physical changes.

197 These relationships, however, are heterogeneous, as the largely stochastic sequence of El Niños
198 and La Niñas shapes the direction and magnitude of damages. Simulations with E-index sums greater than
199 0 (i.e., El Niño-dominated time series) exhibit a negative relationship between ENSO amplitude increases
200 and damages (Fig. 4b, red dots), but the opposite is true for La Niña-dominated time series (blue dots).
201 The same pattern holds for teleconnection changes (Fig. 4c). Critically, because El Niños are stronger
202 than La Niñas, there are many more El Niño- than La Niña-dominated time series. On average, therefore,
203 increases in ENSO amplitude and teleconnections produce large economic losses.

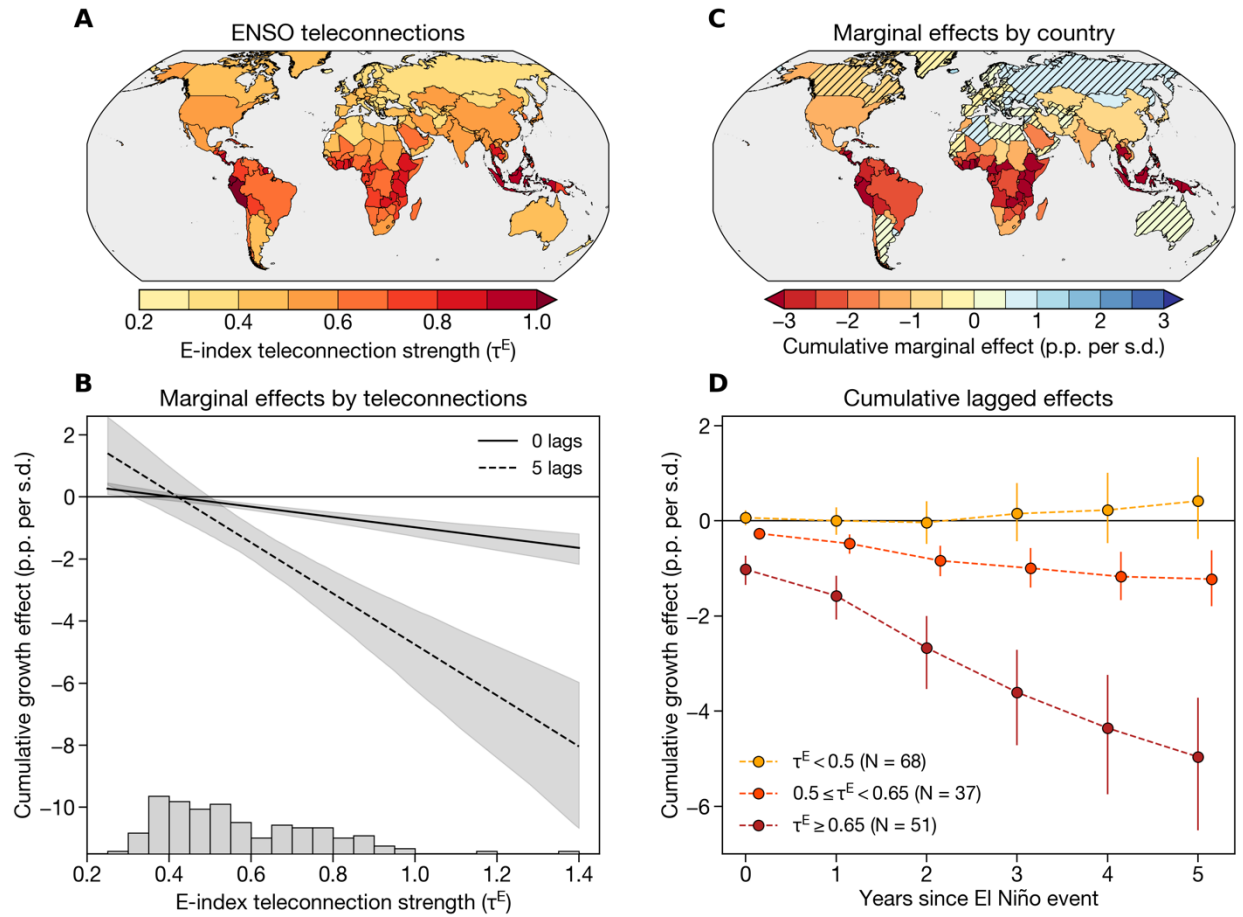
204 Alternative analytical choices, including incorporating C-index changes or holding
205 teleconnections constant, alter the magnitude of losses but do not change the core result of negative
206 damages with warming (Fig. S13). Using only one realization per model increases uncertainty across
207 scenarios (Fig. S13b), highlighting the importance of large ensembles to capture ENSO variability (37).
208 Assuming that damage persistence is permanent substantially increases the magnitude and uncertainty in
209 projected damages (Fig. S13d). Finally, controlling for country-average temperature in our regression
210 does not alter the effect of ENSO (Fig. S14), meaning our results are distinct from temperature-based
211 damage projections (13). ENSO affects sub-national and sub-annual extreme heat or rainfall, and other
212 hazards such as drought, all of which have independent impacts (32, 45, 46).

213 Our findings have implications for climate mitigation and adaptation. All else being equal,
214 increased ENSO amplitude and teleconnections will generate major economic losses not currently
215 included in assessments of climate damages or mitigation benefits. However, the facts that (1) ENSO-
216 driven damages do not depend strongly on emissions scenario (Fig. 4a) and (2) a range of outcomes are
217 possible due to uncertainty in the unique ENSO sequence going forward (Fig. 4b, c) together imply that
218 emissions reductions alone are insufficient to protect economies from El Niño. While mitigation remains
219 critical to blunt the catastrophic impacts of anthropogenic warming (47), our findings also raise the
220 priority of climate adaptation and resilience efforts. Improved disaster risk management and ENSO early
221 warning could reduce ENSO-driven damages (48), and scientific investments in decadal climate
222 prediction could reduce the uncertainty in projections of these damages.

223

224 **Conclusion**

225 Our finding that El Niño has a persistent effect on economic growth has four key implications.
226 Firstly, it demonstrates that growth is highly sensitive to climate variability independent of warming. Our
227 findings demonstrate that the local extreme conditions associated with ENSO integrate into a globally
228 persistent macroeconomic effect, implying large and underestimated costs of historical El Niño events.
229 Secondly, our results demonstrate that future changes to ENSO may increase the macroeconomic costs of
230 warming. Previous climate-economy studies have not incorporated changes in climate variability, and we
231 show that this omission has hidden a potentially major cost of rising temperatures. Thirdly, stochastic
232 variation in ENSO could result in either losses or benefits from warming, emphasizing the importance of
233 investing in ENSO prediction, particularly on decadal time scales (41). Lastly, these findings together
234 suggest that while climate mitigation is essential to reduce accumulating damages from warming, it is
235 imperative to devote more resources to adapting to El Niño in the present day.



236

237

238

239

240

241

242

243

244

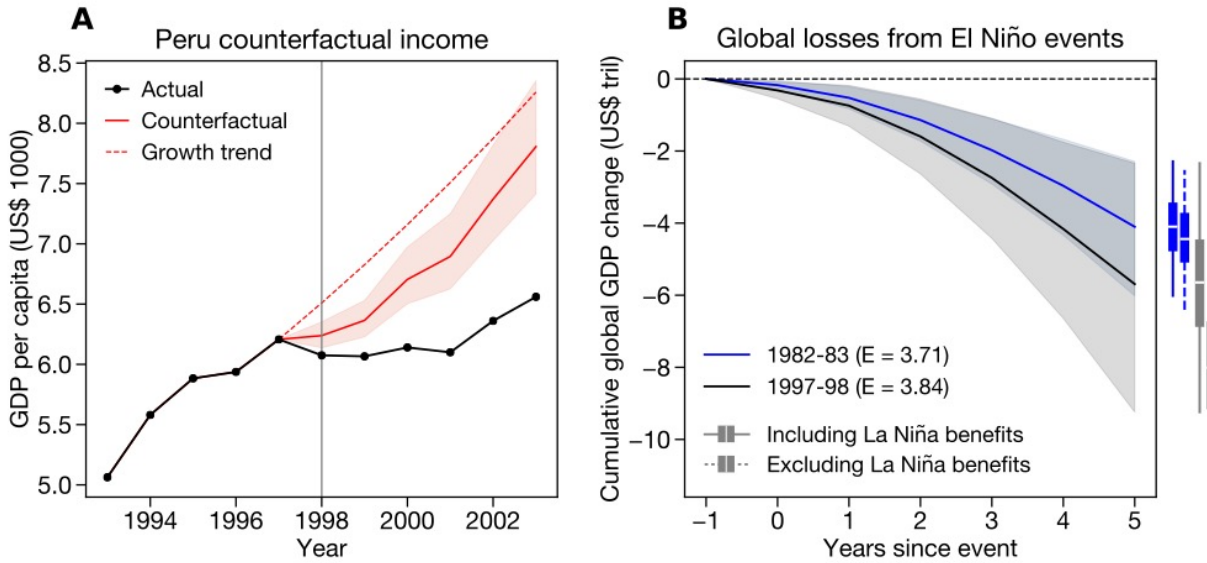
245

246

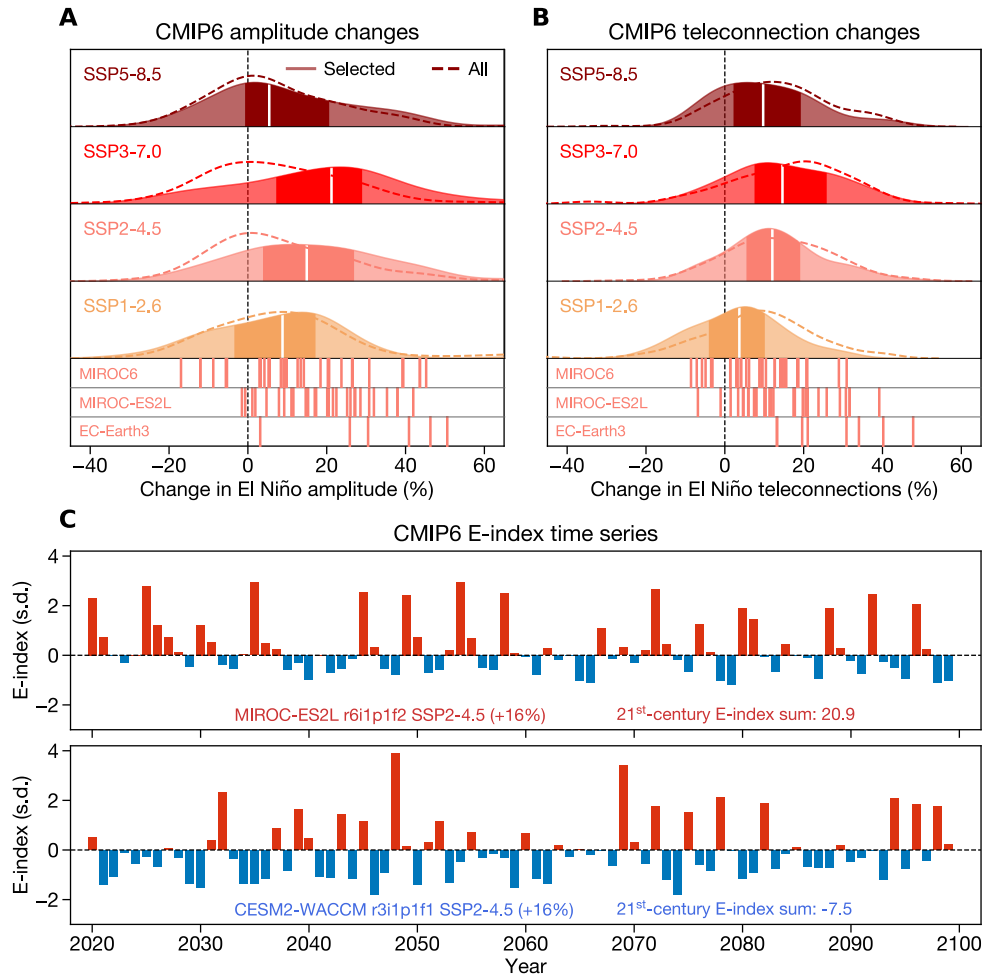
247

248

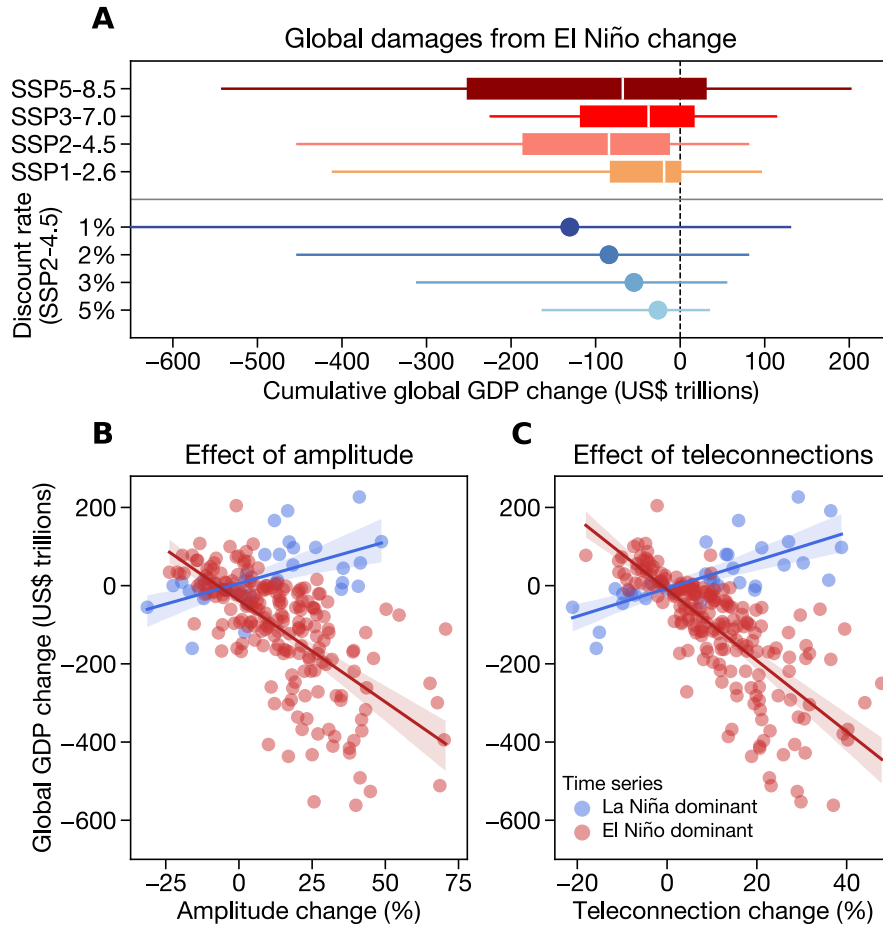
Fig. 1 | Teleconnections mediate the effect of El Niño on economic growth. **A)** Country-level ENSO teleconnections, calculated as the sum of the absolute value of the correlation coefficients between the E-index and monthly country-level temperature and precipitation (Methods). **B)** Marginal effects of El Niño on economic growth across teleconnection values in year of the event (0 lags, solid line) and the fifth year after the event (5 lags, dashed line). Black line shows the mean and shading shows 95% confidence intervals from bootstrap resampling (Methods). Lower histogram shows the density of teleconnection values in the sample. **C)** Cumulative 5-lag effect of El Niño on economic growth for each country. Hatching denotes countries whose effects are not distinguishable from zero (i.e., they fall on a location on the x-axis in (B) where the shading includes zero). **D)** Cumulative effects of El Niño over time, beginning with the year of the event (year 0) and accumulating to the fifth year after the event (year 5). Countries are grouped into three bins according to their teleconnection strength, with “N” denoting the number of countries in each bin. Dots show averages and bars show 95% confidence intervals.



249
 250 **Fig. 2 | Damages from extreme El Niño events.** **A)** GDP per capita (GDPpc) in Peru before and after the
 251 1997-98 El Niño event. Black line shows actual GDPpc, red line shows the average counterfactual
 252 GDPpc across regression bootstrap samples (Methods), and red shading shows 95% confidence interval.
 253 Dashed line shows GDPpc if Peru had maintained its average growth rate from the 5 years preceding the
 254 event. **B)** Cumulative global GDP change for the 5 years after the 1982-83 (blue) and 1997-98 (black) El
 255 Niño events. Center line shows the mean and shading shows the 95% confidence intervals across
 256 regression bootstrap samples. Global GDP change is only calculated for countries with statistically
 257 significant marginal effects (Fig. 1c). Text in legends denotes the DJF-average E-index in the
 258 corresponding years. Boxplots at right show cumulative global GDP change when including the benefits
 259 of the following La Niña events (solid lines) and excluding those benefits (dashed lines). All dollar values
 260 are in constant 2017 prices.



261
 262 **Fig. 3 | Climate model projections of ENSO.** Change in ENSO amplitude (A) and global mean
 263 teleconnection strength (B) between 1940-2019 and 2020-2099 for an ensemble of CMIP6 simulations
 264 from four SSP experiments. In both panels, dashed density lines show changes from all simulations and
 265 solid density plots show amplitude changes from selected high-skill simulations used in the analysis
 266 (Methods). Vertical lines below density plots denote amplitude changes from the individual realizations
 267 of three models (MIROC6, MIROC-ES2L, and EC-Earth3), all drawn from the SSP2-4.5 experiment,
 268 illustrating the wide range of amplitude and teleconnection changes possible from internal variability
 269 alone. C) E-index time series from two example simulations with similar amplitude increases: MIROC-
 270 ES2L r6i1p1f2 (top) and CESM2-WACCM r3i1p1f1 (bottom), both from the SSP2-4.5 experiment. Red
 271 bars denote eastern Pacific El Niño ($E > 0$) and blue bars denote eastern Pacific La Niña ($E < 0$). Left
 272 inset text in each panel denotes the model information and amplitude change. Right inset text denotes the
 273 sum of each E-index time series over the 21st century (2020-99), with positive values indicating that the
 274 time series contains more El Niños than La Niñas and negative values indicating the opposite.



275

276 **Fig. 4 | Global economic impacts of changes in El Niño amplitude and teleconnections. A)** Boxplots
 277 show the cumulative global GDP change in each scenario under a 2% constant discount rate. Colors
 278 correspond to the scenario colors in Fig. 3. In each boxplot, white line denotes the median, box spans the
 279 first and third quartiles, and whiskers span the 95% range. Lower blue lines denote global economic
 280 losses under SSP2-4.5 and a range of discount rates. Dot denotes the median and lines span the 95%
 281 range. **B, C)** Cumulative global GDP change due to changes in ENSO amplitude (**B**) and teleconnections
 282 (**C**) with a 2% discount rate, with each dot corresponding to one climate model simulation. Simulations
 283 are pooled across all four scenarios. Red dots denote simulations in which the 21st-century E-index sum is
 284 greater than 0 (El Niño-dominated time series), while blue dots denote simulations in which the sum is
 285 less than 0 (La Niña-dominated time series). Red and blue regression lines and 95% CIs are drawn
 286 separately for each subset of simulations.

287

288
289
290
291
292
293
294
295
296
297
298
299
300
301
302
303
304
305
306
307
308
309
310



Supplementary Materials for
Persistent Effect of El Niño on Global Economic Growth

Christopher W. Callahan and Justin S. Mankin

correspondence to: Christopher.W.Callahan.GR@dartmouth.edu

This PDF file includes:

- Materials and Methods
- Supplementary Text
- References (49-84)
- Figs. S1 to S17
- Tables S1 to S7

311 **Materials and Methods**

312 Data

313 We use observational climate data from multiple sources: Monthly mean sea surface
314 temperatures (SST) from the HadISST dataset (49), monthly mean atmospheric temperatures
315 from the Berkeley Earth dataset (50), and monthly total precipitation data from the Global
316 Precipitation Climatology Center (51). Temperature and precipitation are aggregated to
317 population-weighted country-level means using year-2000 population data from the Gridded
318 Population of the World (52). We use population weighting to ensure that the spatial aggregation
319 captures climate fluctuations that affect people and economic activity.

320 We use country-level economic data from the Penn World Tables version 10.0 (53),
321 specifically Gross Domestic Product (“RGDPNA”) (in 2017-equivalent dollars) and population
322 (“POP”) for all countries of the world. GDP per capita (GDPpc) is calculated as GDP divided by
323 population. Growth for each year is calculated as the fractional GDPpc change relative to the
324 previous year. Because macroeconomic data may contain measurement error (54), we also repeat
325 the analysis using data from the World Bank World Development Indicators (55), finding similar
326 results (Fig. S4).

327 The time period of analysis for both the teleconnection calculations and regression
328 analysis is 1960-2019, so all observational economic and climate data is limited to that time
329 period.

330 Climate model data come from the sixth phase of the Climate Model Intercomparison
331 Project (56) (CMIP6). We use monthly SST, monthly atmospheric temperature, and daily
332 precipitation data over 1850-2099 from the historical experiment and the four Tier 1 experiments
333 from the Scenario Model Intercomparison Project (57). These four experiments—SSP1-2.6,
334 SSP2-4.5, SSP3-7.0, and SSP5-8.5—span a range of plausible policy futures, from aggressive
335 mitigation (SSP1-2.6) to high emissions (SSP5-8.5) (57, 58). Global mean temperatures rise by
336 ~1.2 °C by 2081-2100 relative to 1995-2014 in the SSP1-2.6 scenario, 2.1 °C in SSP2-4.5, 3.2
337 °C in SSP3-7.0, and 4 °C in SSP5-8.5 (58). Not all models have data available for each
338 experiment, so differences across the experiments are due both to differences in forcing and
339 differences in the sampling of model structure (Tables S3-S6). All climate model data is
340 regridded to a 2°-by-2° grid, using bilinear interpolation from Python’s “xarray” package (59).

341 ENSO indices

343 We use the “E-index” and “C-index” to represent ENSO (9, 27, 36, 60, 61). The E-index
344 represents eastern Pacific El Niño events and captures the nonlinear processes that generate
345 skewness in eastern Pacific SSTs, whereby El Niño events are stronger than La Niña events (9,
346 27). The E-index is a combination of the first two principal components (PCs) of an empirical
347 orthogonal function (EOF) analysis applied to Pacific SSTs (36) over 20 °S – 20 °N and 140 °E
348 – 80 °W, specifically as $E = (PC1 - PC2)/\sqrt{2}$. We calculate the E-index in observations using
349 linearly detrended SST anomalies referenced to 1960-2019 long-term monthly means. We then
350 average the E-index over winter (December-February, DJF), to focus on the season in which
351 ENSO peaks (62); the E-index in year t is therefore defined as the average of the December E-
352 index from year $t-1$ and the January and February indices from year t .

353 The C-index (27) is a companion index to the E-index and is calculated as $C = (PC1 +$
354 $PC2)/\sqrt{2}$. The C-index represents central Pacific La Niña and El Niño events, where La Niña
355 events tend to be stronger than El Niño events. Positive E-index values represent an eastern
356 Pacific El Niño event and negative C-index values represent a central Pacific La Niña event. The

357 E-index and C-index are orthogonal by construction (27), allowing us to include them both in a
358 regression model without a concern for collinearity.

359 To assess the sensitivity of our results to these indices, we also calculate the Niño3 index,
360 defined as linearly detrended SST anomalies averaged over 5 °S – 5 °N and 150 °W – 90 °W.
361 The Niño3 index yields similar, though slightly weaker, results to the E-index (Fig. S4) since it
362 corresponds to eastern Pacific conditions but does not distinguish the spatial structures of El
363 Niño and La Niña.

364 We calculate the DJF E- and C-indices similarly in the CMIP6 models, using
365 quadratically detrended (9) SST anomalies referenced to monthly means from 1850-2014.
366

367 Country-level ENSO teleconnections

368 Our analysis uses a country-specific teleconnection metric to quantify heterogeneity in
369 growth responses according to a country’s geophysical connection to ENSO. To calculate the
370 teleconnection, we first standardize monthly country-level mean temperature and total
371 precipitation by subtracting the long-term (1960-2019) monthly mean and dividing by the long-
372 term monthly standard deviation. We then linearly detrend these standardized anomalies
373 separately for each month to remove the effects of warming and low-frequency climate
374 variability.

375 Next, we correlate these standardized temperature and precipitation time series with the DJF
376 E-index separately for each month m and each country i . El Niño events begin and grow in year
377 $t-1$, peak in the winter, and then decay in the spring and summer of year t , so we allow the DJF
378 E-index to affect both the preceding (beginning just after the “spring predictability barrier” in
379 June of $t-1$) and following years (ending in August of year t) (Fig. S1). We use partial
380 correlations to control for precipitation when analyzing temperature and vice versa to control for
381 the covariance between temperature and precipitation.

382 This calculation yields a distribution of 15 correlation coefficients (one per month from
383 June of year $t-1$ through August of year t) for each country, separately for temperature and
384 precipitation. We then take the three-month running mean of these coefficients across the 15
385 months to smooth out random variation and account for multiple months of exposure to ENSO.
386 Finally, we take the maximum (absolute) correlation coefficients from these running means for
387 both temperature and precipitation and add them together to calculate each country’s E-index
388 teleconnection τ^E . We use absolute values to allow the distinct effects of temperature and
389 precipitation teleconnections to be additive, but our results are robust to considering both
390 positive and negative precipitation teleconnections separately (Fig. S5).

391 This teleconnection metric estimates the degree to which each country’s climate is
392 influenced by ENSO, accounting for: (1) the effects of both temperature and precipitation; (2)
393 multiple sustained months of exposure to ENSO; and (3) the varied timescales on which
394 teleconnections may manifest. Additionally, this strategy allows teleconnections to be defined
395 continuously rather than separating teleconnected and non-teleconnected countries based on
396 arbitrary significance thresholds (8) or previously defined climate zones (19, 20). Fig. S2 shows
397 the steps in this teleconnection calculation, and we perform the same analysis with the C-index to
398 calculate C-index teleconnections (τ^C).
399

400 Econometric analysis

401 The goal of our analysis is to quantify the multi-year effect of ENSO on economic growth.
402 This task requires us to separate ENSO from the other constant and time-varying factors that

403 affect economic growth. We use a distributed lag regression model, estimated with Ordinary
 404 Least Squares, to estimate the effects of eastern Pacific El Niño (the E-index) and central Pacific
 405 La Niña (the C-index) on growth:
 406

$$407 \quad g_{it} = \sum_{L=0}^j [\beta_L E_{t-L} + \Theta_L E_{t-L} * \tau_i^E + \Phi_L C_{t-L} + \Psi_L C_{t-L} * \tau_i^C] + \mu_i + \epsilon_{it} \quad (1)$$

408
 409 Here, g refers to GDPpc growth in country i in time t , E refers to the E-index in year t , and
 410 C refers to the C-index in year t . μ is a country fixed effect, which controls for average
 411 differences between countries such as geography and ensures that our results are identified using
 412 within-country variation in growth. L is the lag at which the coefficient is estimated. The
 413 interactions of E with τ^E and C with τ^C allow the effect of ENSO to differ between countries
 414 based on how strongly coupled each country's climate is to ENSO.

415 The inclusion of lagged terms from years L to j allows us to distinguish between level and
 416 growth effects on the economy. If the effect of El Niño only falls on income levels, then a shock
 417 in year t will be recovered in year $t+1$ as countries rebound to their original income trajectory,
 418 meaning that year $t+1$ will see an abnormally high growth rate. If, instead, El Niño affects the
 419 underlying capacity of the economy to grow, then the years following an event should show
 420 either persistent declines in growth or no change. As such, our analysis focuses on the
 421 cumulative coefficients Ω , which represent the accumulated effect of ENSO in the years after an
 422 event. The interaction of E with country-specific teleconnections τ^E allows us to calculate unique
 423 cumulative effects for each country i and lag length L :
 424

$$425 \quad \Omega_{iL} = \sum_{L=0}^j [\beta_L + \Theta_L * \tau_i^E] \quad (2)$$

426
 427 If Ω_{iL} is indistinguishable from zero, then we cannot reject the hypothesis that El Niño has
 428 only level effects; growth effects are identified if Ω_{iL} is significantly different from zero ($p <$
 429 0.05). Note that the E-index is not highly correlated with itself across lag lengths (Table S7),
 430 meaning that including multiple lags in a single model should not generate multicollinearity.

431 The identifying variation in our model comes from stochastic and unpredictable (30, 63)
 432 shifts in SSTs from year to year, along with the differential effects of those SSTs depending on
 433 teleconnection strength. The E- and C-indices are constant throughout space within a given year,
 434 raising the concern that other time-varying confounders could be correlated with ENSO and
 435 generating spurious results. A typical strategy in empirical climate-economy studies is to include
 436 both unit and time fixed effects in regression models (64), which separate local weather variation
 437 from both time-invariant average conditions and global time-varying shocks. However, because
 438 the E- and C-index terms in Eqn. 1 would be collinear with the year fixed effect, we cannot
 439 estimate our main specification with year effects.

440 We do, however, show results from several alternative models that separate the influence of
 441 ENSO from time-varying confounders. First, adding linear or linear and quadratic country-level
 442 time trends to control for secular trends in technology or demographics does not alter our results
 443 (Fig. S4). Second, bootstrap resampling by year permutes the years in the regression model and
 444 ensures that no single year has a disproportionate influence on the results (Fig. S3). Third,

445 dropping 1983 and 1998 from our data, which were major El Niño events that coincided with
446 financial crises in tropical countries, reduces the magnitude of the effects we find by ~12% but
447 does not alter their statistical or economic significance (Fig. S4). Fourth, we define a unique
448 spatiotemporally varying ENSO index for each country and year by multiplying E_t by τ_i^E .
449 Because this index differs across countries within years, we can estimate the model with country
450 and year fixed effects, and we find negative effects that exceed the results of our main model
451 (Fig. S7). For example, this model predicts that Peru experiences an 8.7-p.p. decline in growth
452 five years after an El Niño, compared to 6.2 p.p. from our original model. Finally, we estimate a
453 discretized version of our main model, where we defined “untreated” countries as countries with
454 $\tau_i^E < 0.5$ and “treated” countries as countries with $\tau_i^E > 0.5$. This allows us to estimate the model
455 with country and year fixed effects, interpreting the discretized interaction term as the effect of
456 ENSO on treated countries. In this case, we find that treated countries experience >3-p.p.
457 declines in growth five years after El Niños, which exceeds the 2.3-p.p. average loss for
458 countries with $\tau_i^E > 0.5$ from our main model (Fig. S7). The inclusion of year fixed effects in
459 these latter two models, along with the other checks we show, supports our conclusion that our
460 results are not driven by time-varying confounders.

461 We estimate confidence intervals by bootstrapping ($N = 1,000$), with countries resampled
462 from a uniform distribution with replacement. Countries are sampled as a block to account for
463 within-country autocorrelation (65). However, alternative bootstrapping schemes yield similar
464 results, such as sampling by year globally or within continents to account for spatial correlation
465 in growth, sampling by continent to account for simultaneous spatial and temporal correlation,
466 and sampling by five-year blocks to account for spatial and short-term temporal correlation (65)
467 (Fig. S3). Multiple forms of clustered parametric standard errors, which are robust to both
468 spatiotemporal autocorrelation in errors and heteroskedasticity across clusters, do not reduce the
469 statistical significance of our results (Table S1, S2).

470 We remove growth values from our sample that are above 18% or below -18%,
471 approximately the 3σ range. We drop 146 values because of this choice, less than 2% of the
472 sample. Including these values does not reduce the average effect, but it does increase the
473 uncertainty (Fig. S4), so we drop these outliers while noting that our results would be similar if
474 we included them.

475 When we estimate separate responses for high-income and low-income countries (Fig.
476 S4), we use the World Bank’s income classifications, grouping low and lower-middle income
477 countries together as well as high and higher-middle income countries. Again, the results accord
478 with our main model.

479 Other time series analysis tools have been used to assess the effect of ENSO such as
480 vector autoregression (VAR) models (18, 21–23) or local projections (18). We use a distributed
481 lag (DL) model for two reasons. Firstly, DL models have been widely used in the empirical
482 climate-economy literature (13, 15, 66, 67), so our approach is consistent with this work.
483 Secondly, VAR models are primarily used in macroeconomic settings where endogeneity is at
484 issue (68). Because ENSO is plausibly exogenous to country-level growth rates, we adopt the
485 more parsimonious DL model.

486 Synthetic data simulations

487 Estimating the effect of El Niño with models that include 14 or more lags results in unstable
488 coefficients and confidence intervals that include zero (Fig. S8). Two plausible interpretations of
489 this result are: (1) that there is no statistically significant growth effect of El Niño after 14 years;
490

491 or (2) that there is a permanent growth effect, but models with many lags cannot confidently
492 identify this effect due to the reduced sample size and increased number of parameters being
493 estimated simultaneously.

494 To examine this issue, we use a perfect model framework where we impute a known El
495 Niño effect to synthetic growth data and then estimate the regression on that data to assess
496 whether we can recover the effect. We construct growth as the combination of a first-order
497 autocorrelated process (AR(1)) with Gaussian noise of mean 0 and s.d. 0.05, a linear trend
498 randomly chosen from a Gaussian distribution of mean 0 and s.d. 0.2 (in p.p. per year), and an El
499 Niño effect. The AR(1) coefficient is set to 0.1, within the range of AR(1) coefficients from the
500 data, and the distribution of trends we choose from is also similar to the distribution of country-
501 level growth trends from the data (Fig. S15).

502 We then create a “true” effect of ENSO on growth and attempt to recover it with the DL
503 model. This predetermined ENSO effect is ultimately arbitrary, but we choose country-level
504 effects that are similar in magnitude to the effects we find in our main regression. We set these
505 effects to accumulate over the first 5 years and plateau at that 5-year value permanently. The
506 non-interacted effect of E is set to sum to 3 p.p. per s.d. and the interaction coefficient with τ is
507 set to sum to -6 p.p. per s.d., meaning that a country with $\tau^E = 1.0$ experiences a cumulative
508 effect of -3.0 p.p. per s.d. ($3 + 1.0 \cdot -6$).

509 We then fit Eqn. 1 using this synthetic growth data and the actual E-index and τ^E values,
510 using between 5 and 18 lags in the regression (beyond 18 lags, the coefficients become
511 undefined as the degrees of freedom decrease). We repeat this entire process 1,000 times for
512 each number of lags, keeping the set El Niño effect constant. Fig. S8 shows the results from
513 these estimations for one example teleconnection value ($\tau^E = 1.0$). These models are generally
514 unbiased, with the central estimate matching the imputed effect. However, confidence intervals
515 steadily grow as lags are added. With 14 or more lags, the coefficients become statistically
516 insignificant. These results demonstrate that even with a known permanent effect of El Niño,
517 estimating additional lag terms induces sufficient uncertainty to yield insignificant coefficients.
518 To assume that El Niño has no effect in the 14-lag model therefore risks a Type II error. That
519 being said, as a conservative choice in our historical attribution and in our damage projections,
520 we only allow the effects to be partially persistent rather than permanently persistent (see
521 *Economic damages from changes to ENSO*). In our attribution of the costs of the 1982-83 and
522 1997-98 events, we estimate costs accumulating to 5 years after the event. In our projections, we
523 allow effects to accumulate to 14 years, the maximum length we can confidently identify effects
524 from the observational data (Fig. S8). In a sensitivity test, we allow the effects to be permanent
525 (Fig. S13).

526

527 Economic damages from historical extreme El Niño events

528 The regression coefficients derived from Eqn. 1, β and θ , provide estimates of the change
529 in economic growth for a 1-s.d. change in the E-index. These coefficients can then be applied to
530 actual and hypothetical E-index time series to calculate the growth effects of specific historical
531 El Niño events. Here we focus on the two major El Niño events of 1982-83 and 1997-98. We
532 develop “counterfactual” E-index time series wherein these events did not occur by setting the
533 corresponding E-index values (1983 and 1998) to zero. We then apply the regression coefficients
534 to the actual and counterfactual time series to calculate the growth difference between them over
535 the five years after the event. Formally, if E^O represents the observed E-index in the year of the

536 event (t), and E^{CF} represents the counterfactual E-index in that year, we calculate the growth
537 change in country i from year t through year $t+L$ as:

538
539
$$\Delta g_{i(t+L)} = [\beta_L E_t^{CF} + \Theta_L E_t^{CF} * \tau_i^E] - [\beta_L E_t^O + \Theta_L E_t^O * \tau_i^E] \quad (3)$$

540
541 We add these growth change values to the observed growth data, yielding a counterfactual
542 growth time series, and we integrate counterfactual growth to calculate counterfactual income
543 from the year of the event to 5 years after the event. Losses due to each event are calculated as
544 the difference between observed and counterfactual income. Details of this procedure can be
545 found in Diffenbaugh and Burke (69).

546 Note that E^{CF} is zero in our analysis, so the first bracketed term on the right-hand-side of
547 Eqn. 3 is zero, but we provide the full equation because it generalizes to other counterfactual E-
548 index values.

549 The above analysis only incorporates reductions in growth due to the El Niño events.
550 However, because El Niño events can dynamically trigger La Niña events (34), which have
551 beneficial effects (Fig. S10), a full accounting of the effects of El Niño should incorporate these
552 offsetting beneficial events. The 1982-83 El Niño may have triggered the La Niña of 1984-85
553 (while the C-index was only -0.07 in 1984, it was -1.1 in 1985), and the 1997-98 El Niño may
554 have triggered the major La Niña of 1999-2000 (the C-index was -2.1 in 1999 and -2.0 in 2000).
555 We incorporate these beneficial effects for both El Niño events by setting the C-index values for
556 the following two years (i.e., 1999 and 2000 in the case of the 1998 El Niño) to zero and
557 calculating the growth difference between the actual and counterfactual C-index time series. The
558 total growth change over the five years following the El Niño event is therefore the reduction due
559 to the El Niño event plus the increase due to the following La Niña events.

560 For both events, we limit our analysis to countries with continuous GDPpc data since
561 1982 to ensure that the same countries are included in both calculations. This restriction means
562 that nations with short GDPpc records (e.g., post-Soviet nations like Ukraine) are not included in
563 these calculations.

564 565 Climate model selection

566 Many climate models do not realistically represent the physical processes that drive
567 ENSO (70–72). To ensure that our projections are physically realistic, we filter the simulations
568 we use based on criteria set out in previous studies (9, 36, 72). We calculate a parameter known
569 as α from each model, which is the quadratic coefficient on the relationship between the first and
570 second principal components from the EOF analysis used to calculate the E-index and C-index
571 (72) (see *ENSO indices*).

572 The observed value of α is -0.34, indicating a strong nonlinearity in the principal
573 component space and a strong differentiation between eastern Pacific and central Pacific El Niño
574 events. Models which simulate an α value closer to the observed value also more effectively
575 represent the variance and skewness in SST anomalies, as well as the distinct eastern and central
576 Pacific El Niño phases (9, 72). We follow Cai et al. (9) in selecting all models with α at least
577 50% of the observed value, meaning -0.17 or less. Tables S3-S6 show the total and selected
578 realizations for each experiment. We also test the sensitivity of our results to using only one
579 realization from each model (Fig. S13).

580 581 ENSO amplitude and teleconnections in climate models

582 We define ENSO amplitude as the standard deviation of the quadratically detrended E-
 583 index (9, 42). We calculate each climate model simulation’s amplitude in the historical period,
 584 which we define as 1940-2019 to parallel the observational data, and in the future, which we
 585 define as 2020-2099. The 1940-2019 historical period is chosen so that the historical period is
 586 the same length as the future period.

587 We calculate model-based ENSO teleconnections using the same method as the
 588 observations. We perform this calculation separately for the historical and future periods,
 589 standardizing and linearly detrending each country’s temperature and precipitation time series
 590 independently for each period. This method removes mean shifts due to global warming or low-
 591 frequency variability and allows us to isolate the interannual signal of ENSO.

592 Economic damages from changes to ENSO

594 Calculating economic damages from warming-driven ENSO changes requires a
 595 counterfactual world where ENSO evolves without rising temperatures. We calculate the
 596 counterfactual ENSO time series for each simulation by re-scaling its future time series to have
 597 the amplitude that simulation had in the historical period. For example, if E-index amplitude
 598 increases by 20% for a given model realization, we calculate its counterfactual E-index time
 599 series by multiplying its future time series by 0.8 (i.e., $0.8 = 1 - 0.2$). This method preserves the
 600 particular sequence of El Niño and La Niña events in the future, since this sequence is assumed
 601 to be unforced (Fig. S12), but eliminates the forced change in ENSO amplitude.

602 We calculate counterfactual ENSO teleconnections with a similar “delta method.” For
 603 each country in each model, we calculate the change in teleconnection value between the
 604 historical and future simulations. We then add this change to each country’s observed
 605 teleconnection value to implicitly bias-correct the model output. The “counterfactual”
 606 teleconnections are thus equal to the observed values and the “future” teleconnections are the
 607 observed-plus-change values.

608 We then calculate the economic effects of changes to ENSO by comparing the future and
 609 counterfactual time series and teleconnections from each model. For each year t between 2020
 610 and 2099, we calculate the growth change from year t to year $t+5$ as the difference between the
 611 future and counterfactual time series and teleconnections:

$$612 \Delta g_{i(t+L)} = [\beta_L E_t^{CF} + \Theta_L E_t^{CF} * \tau_i^{CF}] - [\beta_L E_t^F + \Theta_L E_t^F * \tau_i^F] \quad (4)$$

615 Here, E^F refers to the future E-index time series and E^{CF} refers to the counterfactual E-index
 616 time series. Similarly, τ^F refers to future teleconnections and τ^{CF} refers to counterfactual
 617 teleconnections. This calculation yields a growth change time series where each value is the
 618 combined effect of the contemporaneous and lagged effects. We then calculate economic growth
 619 caused by changes in ENSO by subtracting these growth change values from the SSP income
 620 growth projections and integrating growth to calculate income; the new time series represent the
 621 deviations from the SSP baselines caused by changes in ENSO amplitude. Damages are
 622 calculated as the difference between this new time series and the SSP baseline. Details of this
 623 procedure can be found in Burke et al. (13). We perform an analogous calculation using the C-
 624 index time series and teleconnections to calculate C-index damages.

625 We note that this procedure calculates counterfactual income as accumulated over the entire
 626 21st century, rather than preceding specific events such as in Fig. 2. This distinction is because
 627 these two methods are aimed at answering different questions. In Fig. 2, we are interested in the

628 effects of specific El Niño events, whereas in Fig. 4, we are interested in the accumulated effect
629 of human-caused changes in ENSO over the 21st century.

630 Finally, given the rebound effects observed after ~10 lags, as well as the large
631 uncertainties in models including longer lags (Fig. S8), we adopt a conservative approach to
632 damage persistence in these calculations. Because we cannot confidently identify permanent
633 effects after 14 years, we allow the growth effect of ENSO to rebound to zero 14 years after the
634 event, meaning that each El Niño affects the global economy for 15 years total (14 lags plus a
635 contemporaneous effect). We do this by applying Eqn. 4 for the first six years (year 0 through
636 year 5) using the coefficients from the main 5-lag model, then allowing the effect to plateau for
637 years 6 through 8, then reversing those coefficients and allowing economies to rebound from
638 years 9 through 14. Thus, while we prevent El Niño events from having more than 15 years of an
639 effect, this does not mean that their effect is zero; an affected country has lost substantial
640 economic output during those 15 years that is never recovered. Fig. S16 illustrates this
641 schematically. In a sensitivity analysis, we show results if we assume that damages are
642 permanent and never recovered, a choice which yields substantially greater losses as well as
643 greater uncertainty in those losses (Fig. S13d).

644

645 **Supplementary Text**

646 Regression-based teleconnections

647 Our main analysis uses a correlation coefficient to calculate teleconnections, but we also
648 assess the sensitivity of this choice by using partial regression coefficients instead. Using a
649 regression coefficient leads Peru and Ecuador to be strong outliers from the rest of the
650 distribution (fig. S4e), with values at or above 2. Estimating the growth regression with these
651 values leads to large uncertainties as Peru and Ecuador have an outsized influence on the
652 regression (fig. S4e), so the correlation coefficient is a more stable metric for use in the growth
653 regression. However, we emphasize that the effect of El Niño is still strong and statistically
654 significant when using regression coefficients (Fig. S4e), so our results are not an artifact of the
655 choice to use the correlation coefficient.

656

657 Temperature- or precipitation-based teleconnections

658 Our main analysis defines teleconnections using the combination of temperature and
659 precipitation correlations. We can also define teleconnections solely based on the temperature or
660 precipitation portions of the calculation, similar to previous studies that have focused on
661 temperature to define teleconnections (6, 8). Results for this sensitivity analysis are shown in
662 Fig. S5. The temperature-based estimate is similar to that from both temperature and
663 precipitation, but the effect is weaker with precipitation alone. Our interpretation is that
664 aggregating the data to the monthly time scale and country spatial scale dampens the signal of
665 precipitation more than it does temperature. Consistent with this interpretation, empirical
666 climate-economy studies tend to find little effect of precipitation on country-level growth (13,
667 16).

668

669 Cumulative teleconnections

670 By using the maximum of three-month running means, our main teleconnection analysis
671 focuses on countries' short-term extreme exposure to ENSO rather than capturing cumulative
672 exposure over the entire ENSO life cycle. An alternative teleconnection metric which uses the

673 sum of statistically significant ($p < 0.05$) correlation coefficients across the 15 months for each
674 country yields very similar results, with high correlations between this and our original metric
675 and nearly identical marginal growth effects (fig. S5). This analysis implies that focusing on the
676 few months of maximum exposure is sufficient to capture the effects of ENSO on economies
677 broadly.

678 679 Heterogeneity in historical teleconnections

680 Our main analysis treats teleconnections as constant in time in the observational period.
681 However, sampling variability and changes in ENSO behavior (among other things) may result
682 in temporal heterogeneity in teleconnections. Fig. S17 shows teleconnections calculated in
683 rolling 30-windows over the historical period. Temporal variation is apparent, at least partly due
684 to the shorter time period used to calculate these teleconnections. However, the distribution of
685 teleconnection values is relatively stable, and the average country experiences temporal variation
686 of only about 13% of its mean value. As such, we use the teleconnection values calculated across
687 the entire time period in our main analysis, though we do allow teleconnections to change with
688 forcing in our climate model analysis.

689 Finally, a key consideration in empirical climate-economy studies is the need to
690 aggregate physical variables to the country scale, which is not a geophysically meaningful scale.
691 To understand the implications of this aggregation, we re-calculate E-index teleconnections at
692 the gridded scale (fig. S17). Teleconnections can vary across grid cells, but the average country
693 only experiences within-country spatial variation of about 11% of its mean teleconnection value
694 (fig. S17). Furthermore, population-weighted country-average grid-cell teleconnection values are
695 similar to the original teleconnection values calculated from country-average temperature and
696 precipitation (fig. S17), implying that subnational spatial variation in ENSO teleconnections does
697 not substantially affect our results.

698 699 Relationship between our work and recent differences-in-differences literature

700 Our empirical framework is very similar to typical “differences-in-differences” (DID)
701 approaches in economics, involving a treatment variable that varies over time (E and C) and a
702 cross-sectional variable that denotes treatment status (τ). A series of recent papers have
703 illustrated problems with traditional DID approaches, especially when treatment effects are
704 heterogeneous in time and space and treatment timing is staggered (73–75). This type of research
705 design can produce inappropriate comparisons between already treated and newly treated units,
706 resulting in average treatment effect estimates that differ in magnitude and sign from the true
707 effects. While novel estimators have been proposed to avoid these problems (76–78), this
708 literature is still emerging and it is not clear that such estimators are designed for settings with
709 continuous treatments that vary year-to-year and have dynamic effects (79). In lieu of using an
710 alternative estimator, we run several robustness tests to examine the heterogeneity of the effects
711 of ENSO over time and space, which can indicate whether our results are biased by this
712 heterogeneity (80). We estimate the effect in rolling thirty-year windows over the 1960-2019
713 sample period, after dropping individual countries, and after dropping individual years (Fig. S6).
714 In all cases, these estimates are quite similar to our main effect, indicating that unmodeled
715 treatment effect heterogeneity should not pose a threat to our main analysis.

716 717 Value of climate model selection

718 Our climate model selection criterion preserves the benefit of a multi-model ensemble,
719 allowing us to sample structural uncertainty in model representation of ENSO as well as initial-
720 condition uncertainty, while incorporating information about model skill (81). Treating all
721 simulations in a multi-model ensemble equally has been criticized for assuming that all
722 simulations are independent samples that represent the climate system with equal skill (82),
723 especially since CMIP is an ensemble of opportunity rather than a systematic sampling of
724 uncertainty space. Our consideration of model skill provides an ensemble estimate that is likely
725 more accurate than could be achieved without such consideration. Other methods such as bias
726 correction (83, 84) could also improve ensemble skill, but we use the simpler selection criterion
727 based on α given its consistency with the E- and C-indices and its use in the ENSO modeling
728 community.

729

730 Sensitivity of damages calculation to alternative choices

731 We incorporate both amplitude and teleconnection changes in our damage projections.
732 Holding teleconnections constant reduces both the magnitude and uncertainty of the damage
733 projections, though they remain negative on average and negatively skewed (fig. S13). Further, a
734 key assumption in these calculations is that the β and θ coefficients (Eqn. 1) remain consistent at
735 a given teleconnection level between the past and future, though individual countries' actual
736 teleconnections may change. This assumption would be violated if societies undertook
737 adaptation measures in response to changes in ENSO amplitude or teleconnections to reduce
738 their sensitivity to ENSO, which is why the need for increased adaptation is a key theme in our
739 results.

740 Finally, our damages calculations use as many simulations from each model as possible
741 (Tables S3-S6) to sample both model structural differences and differences in outcomes due to
742 internal climate variability. Using only the first simulation from each model can generate
743 different results; for example, the SSP5-8.5 simulation yields benefits and SSP1-2.6 yields
744 stronger losses. However, we emphasize that—conditional on our model selection criterion—all
745 selected simulations from a given model are physically plausible given the forcing and boundary
746 conditions. Therefore, the results we present in Fig. 4 are a more complete accounting of the
747 possible effects of ENSO changes.

748

749 **References**

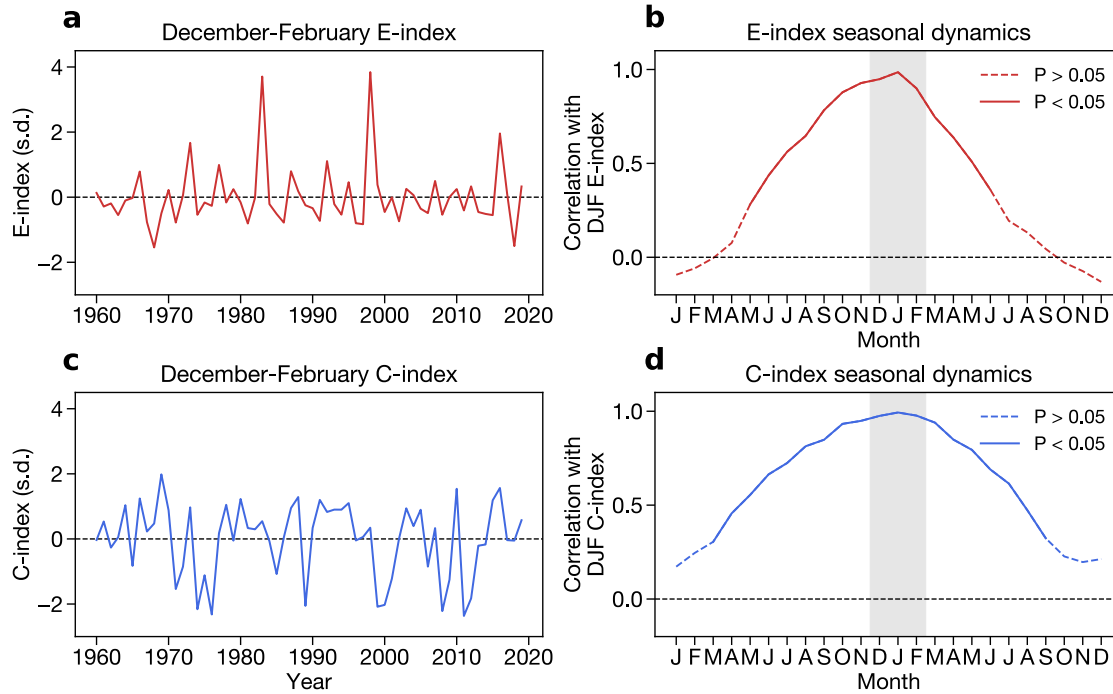
750

- 751 49. N. A. Rayner, D. E. Parker, E. B. Horton, C. K. Folland, L. V. Alexander, D. P. Rowell, E. C. Kent,
752 A. Kaplan, Global analyses of sea surface temperature, sea ice, and night marine air temperature
753 since the late nineteenth century. *J. Geophys. Res. Atmospheres*. **108** (2003),
754 doi:10.1029/2002JD002670.
- 755 50. R. A. Rohde, Z. Hausfather, The Berkeley Earth Land/Ocean Temperature Record. *Earth Syst. Sci.*
756 *Data Discuss.*, 1–16 (2020).
- 757 51. U. Schneider, A. Becker, P. Finger, A. Meyer-Christoffer, B. Rudolf, M. Ziese, GPCP full data
758 reanalysis version 6.0 at 0.5: monthly land-surface precipitation from rain-gauges built on GTS-
759 based and historic data. *GPCP Data Rep Doi*. **10** (2011).

- 760 52. C. U. Center for International Earth Science Information Network CIESIN, *Gridded Population of*
761 *the World, Version 4 (GPWv4): Population Count* (2016).
- 762 53. R. C. Feenstra, R. Inklaar, M. P. Timmer, The next generation of the Penn World Table. *Am. Econ.*
763 *Rev.* **105**, 3150–82 (2015).
- 764 54. A. Deaton, A. Heston, Understanding PPPs and PPP-Based National Accounts. *Am. Econ. J.*
765 *Macroecon.* **2**, 1–35 (2010).
- 766 55. T. W. Bank, *World Development Indicators 2016* (2016).
- 767 56. V. Eyring, S. Bony, G. A. Meehl, C. A. Senior, B. Stevens, R. J. Stouffer, K. E. Taylor, Overview of
768 the Coupled Model Intercomparison Project Phase 6 (CMIP6) experimental design and
769 organization. *Geosci. Model Dev.* **9**, 1937–1958 (2016).
- 770 57. B. C. O’Neill, C. Tebaldi, D. P. van Vuuren, V. Eyring, P. Friedlingstein, G. Hurtt, R. Knutti, E.
771 Kriegler, J.-F. Lamarque, J. Lowe, G. A. Meehl, R. Moss, K. Riahi, B. M. Sanderson, The Scenario
772 Model Intercomparison Project (ScenarioMIP) for CMIP6. *Geosci. Model Dev.* **9**, 3461–3482
773 (2016).
- 774 58. C. Tebaldi, K. Debeire, V. Eyring, E. Fischer, J. Fyfe, P. Friedlingstein, R. Knutti, J. Lowe, B.
775 O’Neill, B. Sanderson, D. van Vuuren, K. Riahi, M. Meinshausen, Z. Nicholls, K. B. Tokarska, G.
776 Hurtt, E. Kriegler, J.-F. Lamarque, G. Meehl, R. Moss, S. E. Bauer, O. Boucher, V. Brovkin, Y.-H.
777 Byun, M. Dix, S. Gualdi, H. Guo, J. G. John, S. Kharin, Y. Kim, T. Koshiro, L. Ma, D. Olivié, S.
778 Panickal, F. Qiao, X. Rong, N. Rosenbloom, M. Schupfner, R. Séférian, A. Sellar, T. Semmler, X.
779 Shi, Z. Song, C. Steger, R. Stouffer, N. Swart, K. Tachiiri, Q. Tang, H. Tatebe, A. Voltaire, E.
780 Volodin, K. Wyser, X. Xin, S. Yang, Y. Yu, T. Ziehn, Climate model projections from the Scenario
781 Model Intercomparison Project (ScenarioMIP) of CMIP6. *Earth Syst. Dyn.* **12**, 253–293 (2021).
- 782 59. S. Hoyer, J. Hamman, xarray: N-D labeled arrays and datasets in Python. *J Open Res Softw. Revis.*
783 (2017).
- 784 60. F. Jia, W. Cai, B. Gan, L. Wu, E. Di Lorenzo, Enhanced North Pacific impact on El Niño/Southern
785 Oscillation under greenhouse warming. *Nat. Clim. Change*, 1–8 (2021).
- 786 61. B. Ng, W. Cai, T. Cowan, D. Bi, Impacts of Low-Frequency Internal Climate Variability and
787 Greenhouse Warming on El Niño–Southern Oscillation. *J. Clim.* **34**, 2205–2218 (2021).
- 788 62. E. Tziperman, M. A. Cane, S. E. Zebiak, Y. Xue, B. Blumenthal, Locking of El Niño’s Peak Time to
789 the End of the Calendar Year in the Delayed Oscillator Picture of ENSO. *J. Clim.* **11**, 2191–2199
790 (1998).
- 791 63. M. Newman, P. D. Sardeshmukh, Are we near the predictability limit of tropical Indo-Pacific sea
792 surface temperatures? *Geophys. Res. Lett.* **44**, 8520–8529 (2017).
- 793 64. C. D. Kolstad, F. C. Moore, Estimating the economic impacts of climate change using weather
794 observations. *Rev. Environ. Econ. Policy.* **14**, 1–24 (2020).
- 795 65. M. Burke, W. M. Davis, N. S. Diffenbaugh, Large potential reduction in economic damages under
796 UN mitigation targets. *Nature.* **557** (2018).

- 797 66. S. M. Hsiang, A. S. Jina, The causal effect of environmental catastrophe on long-run economic
798 growth: Evidence from 6,700 cyclones. *Natl. Bur. Econ. Res. Work. Pap.* (2014).
- 799 67. S. Hsiang, Climate econometrics. *Annu. Rev. Resour. Econ.* **8**, 43–75 (2016).
- 800 68. J. H. Stock, M. W. Watson, Vector Autoregressions. *J. Econ. Perspect.* **15**, 101–115 (2001).
- 801 69. N. S. Diffenbaugh, M. Burke, Global warming has increased global economic inequality. *Proc. Natl.*
802 *Acad. Sci.* **116**, 9808–9813 (2019).
- 803 70. E. Guilyardi, A. Wittenberg, A. Fedorov, M. Collins, C. Wang, A. Capotondi, G. J. van Oldenborgh,
804 T. Stockdale, Understanding El Niño in Ocean–Atmosphere General Circulation Models: Progress
805 and Challenges. *Bull. Am. Meteorol. Soc.* **90**, 325–340 (2009).
- 806 71. R. Seager, M. Cane, N. Henderson, D.-E. Lee, R. Abernathey, H. Zhang, Strengthening tropical
807 Pacific zonal sea surface temperature gradient consistent with rising greenhouse gases. *Nat. Clim.*
808 *Change.* **9**, 517–522 (2019).
- 809 72. C. Karamperidou, F.-F. Jin, J. L. Conroy, The importance of ENSO nonlinearities in tropical pacific
810 response to external forcing. *Clim. Dyn.* **49**, 2695–2704 (2017).
- 811 73. A. C. Baker, D. F. Larccker, C. C. Y. Wang, How much should we trust staggered difference-in-
812 differences estimates? *J. Financ. Econ.* **144**, 370–395 (2022).
- 813 74. C. de Chaisemartin, X. D’Haultfoeuille, Two-Way Fixed Effects and Differences-in-Differences with
814 Heterogeneous Treatment Effects: A Survey (2022), , doi:10.3386/w29691.
- 815 75. J. Roth, P. H. C. Sant’Anna, A. Bilinski, J. Poe, What’s Trending in Difference-in-Differences? A
816 Synthesis of the Recent Econometrics Literature (2023), , doi:10.48550/arXiv.2201.01194.
- 817 76. B. Callaway, P. H. C. Sant’Anna, Difference-in-Differences with multiple time periods. *J. Econom.*
818 **225**, 200–230 (2021).
- 819 77. B. Callaway, A. Goodman-Bacon, P. H. C. Sant’Anna, Difference-in-Differences with a Continuous
820 Treatment (2021), , doi:10.48550/arXiv.2107.02637.
- 821 78. C. de Chaisemartin, X. D’Haultfoeuille, Two-Way Fixed Effects Estimators with Heterogeneous
822 Treatment Effects. *Am. Econ. Rev.* **110**, 2964–2996 (2020).
- 823 79. C. de Chaisemartin, X. D’Haultfoeuille, F. Pasquier, G. Vazquez-Bare, Difference-in-Differences
824 Estimators for Treatments Continuously Distributed at Every Period (2022), ,
825 doi:10.48550/arXiv.2201.06898.
- 826 80. P. Jakiela, Simple Diagnostics for Two-Way Fixed Effects (2021), , doi:10.48550/arXiv.2103.13229.
- 827 81. R. Knutti, J. Sedláček, B. M. Sanderson, R. Lorenz, E. M. Fischer, V. Eyring, A climate model
828 projection weighting scheme accounting for performance and interdependence. *Geophys. Res. Lett.*
829 **44**, 1909–1918 (2017).
- 830 82. R. Knutti, The end of model democracy? *Clim. Change.* **102**, 395–404 (2010).

- 831 83. P. Huang, J. Ying, A Multimodel Ensemble Pattern Regression Method to Correct the Tropical
832 Pacific SST Change Patterns under Global Warming. *J. Clim.* **28**, 4706–4723 (2015).
- 833 84. D. Chen, M. A. Cane, S. E. Zebiak, R. Cañizares, A. Kaplan, Bias correction of
834 an ocean-atmosphere coupled model. *Geophys. Res. Lett.* **27**, 2585–2588 (2000).

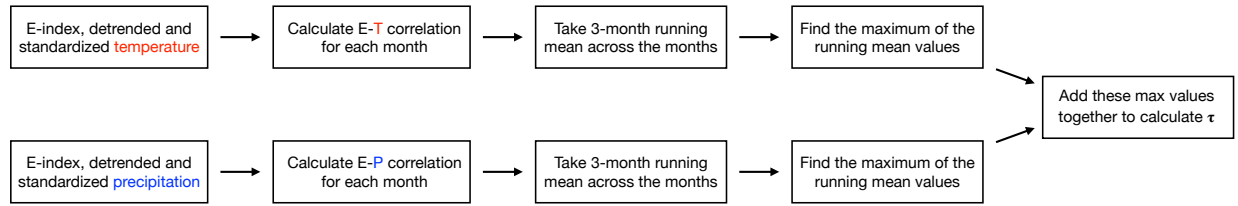


835

836 **Fig. S1.**

837 Interannual and seasonal dynamics of the E- and C-index. A) Timeseries of the average E-index
 838 over December, January, and February (DJF) of each year, where the values are referenced to the
 839 year of January and February. B) Pearson correlation coefficient between the E-index in each
 840 month and the DJF-mean E-index. Solid lines denote correlation coefficients that are statistically
 841 significant ($p < 0.05$) and dashed lines denote correlation coefficients that are statistically
 842 insignificant ($p > 0.05$). C) As in (A), but for the DJF C-index. D) As in (B), but for the DJF C-
 843 index.

844

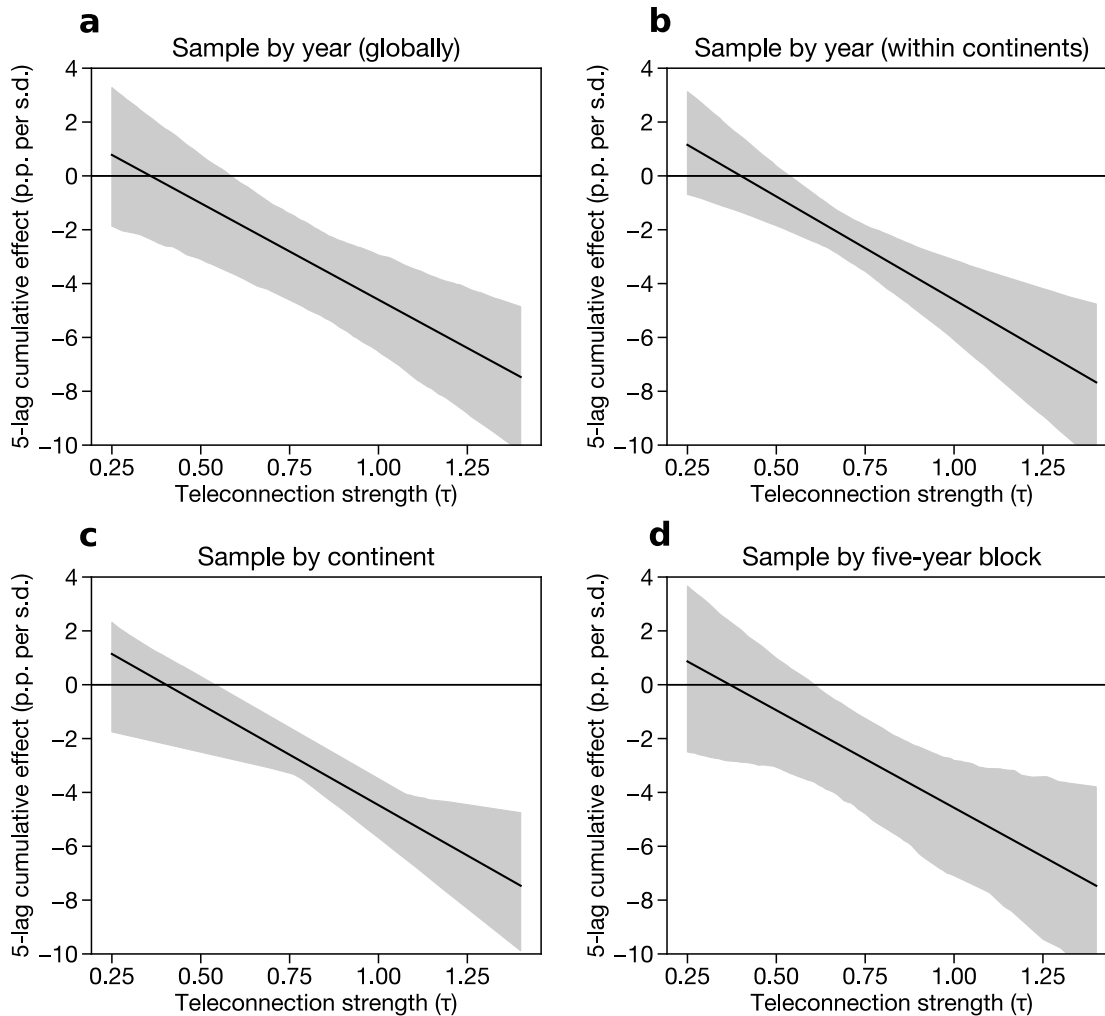


845

846 **Fig. S2**

847 Flow chart for calculation of country-level E-index teleconnections. An analogous calculation is
 848 made for C-index teleconnections.

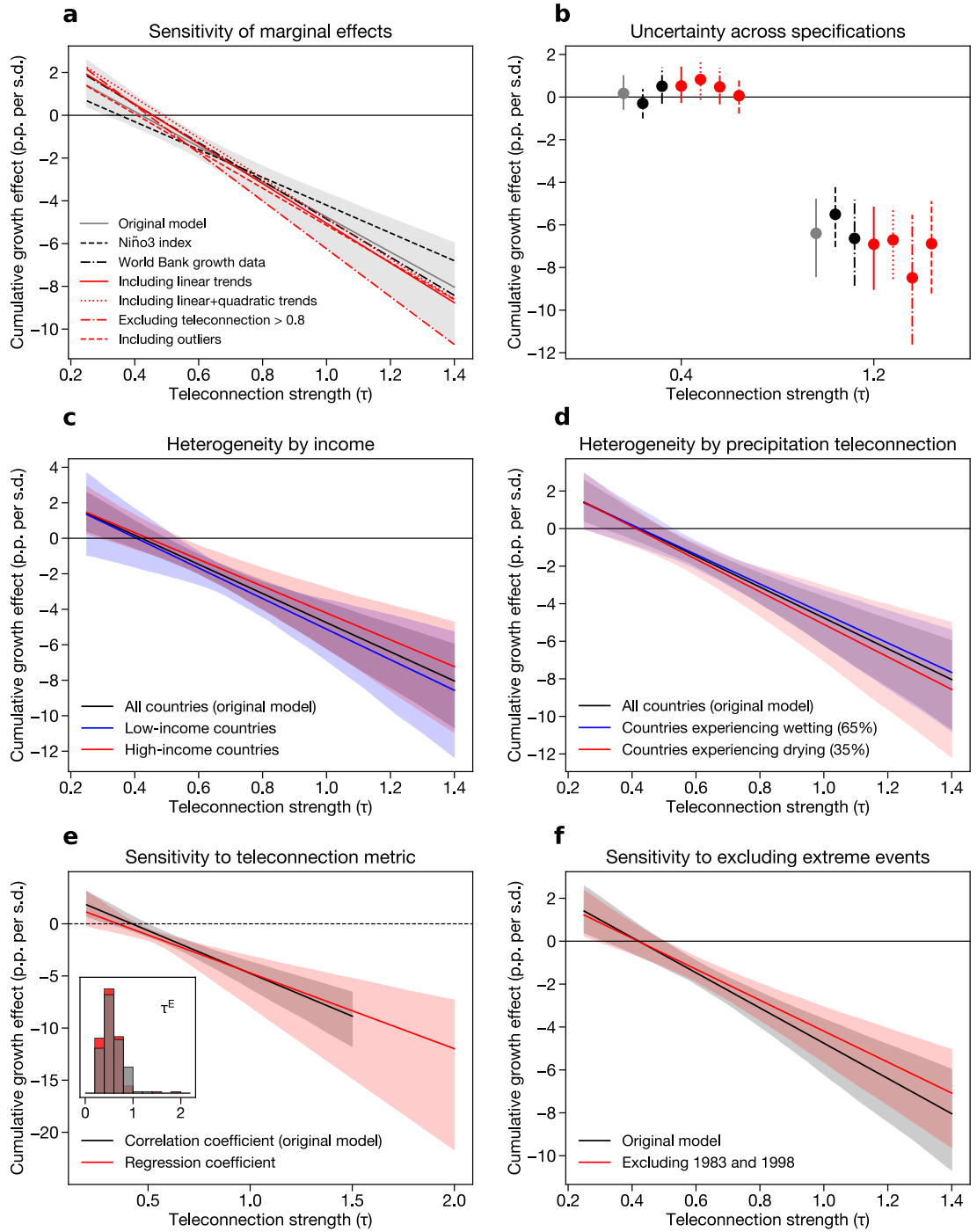
849



850

851 **Fig. S3**

852 Regression results using alternative bootstrap sampling schemes. A) Cumulative 5-lag effect of
 853 ENSO on economic growth when sampling by year, keeping all countries from a given year
 854 together, to account for global spatial correlation in growth within a given year. B) Effect when
 855 sampling by continent-year combinations to account for spatial correlation in growth within
 856 specific continents in a given year. C) Effect when sampling by continents to account for
 857 simultaneous within-continent temporal and spatial correlation in growth. D) Effect when
 858 sampling by five-year blocks to account for global spatial correlation in growth and short-term
 859 (i.e., five-year) temporal correlation in growth. In all cases, solid line shows the mean and
 860 shading shows the 95% confidence intervals. All samples are taken from uniform distributions
 861 with replacement. All axes are the same ranges across panels.

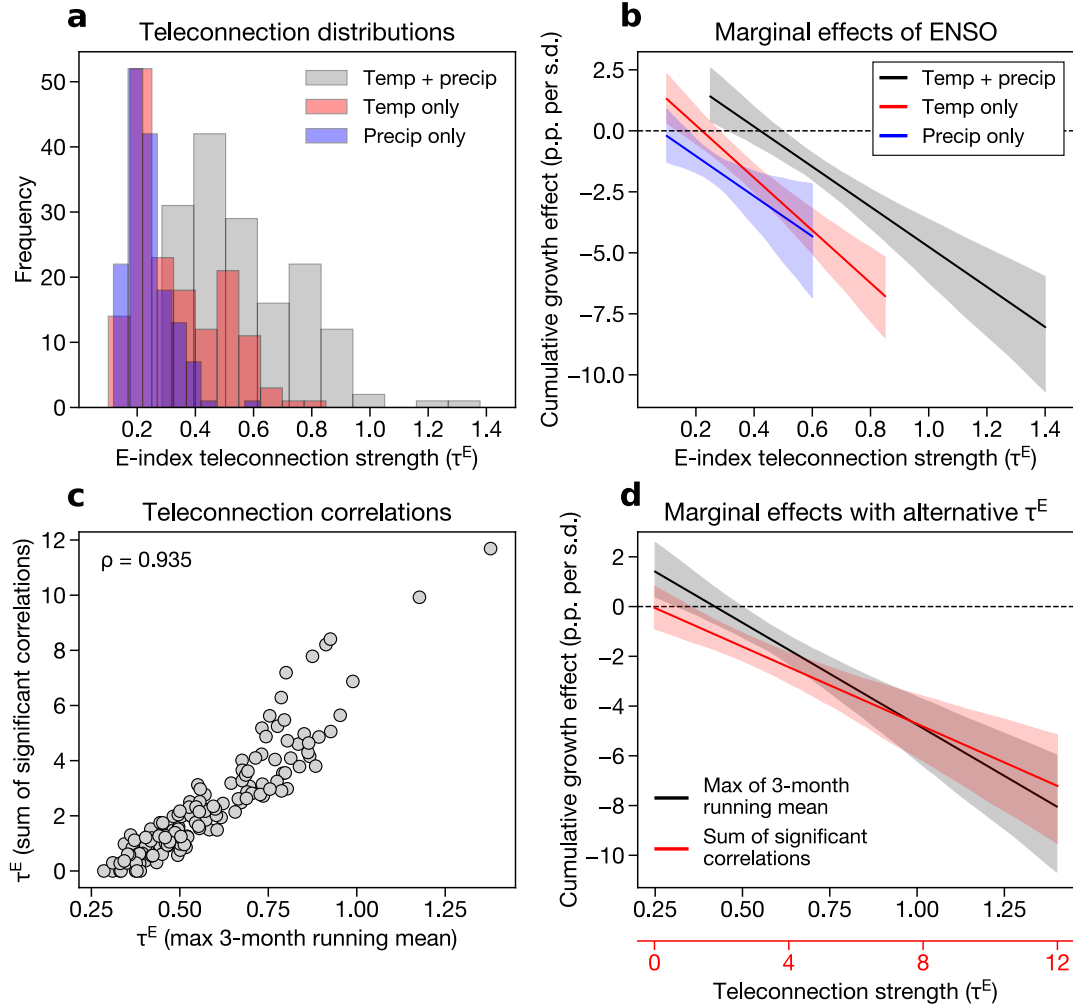


862

863 **Fig. S4**

864 Sensitivity and heterogeneity of the effect of El Niño. A) Cumulative 5-lag effect of El Niño on
 865 growth across a range of specifications: the main model (gray line shows mean and shading
 866 shows 95% confidence intervals), a model using the Niño3 index instead of the E- and C-index
 867 (black dashed line), a model using World Bank growth data instead of the Penn World Tables
 868 (black dash-dot line), a model that includes a country-specific linear trend in growth (red solid
 869 line), a model that includes both linear and quadratic country-specific trends (red dotted line), a

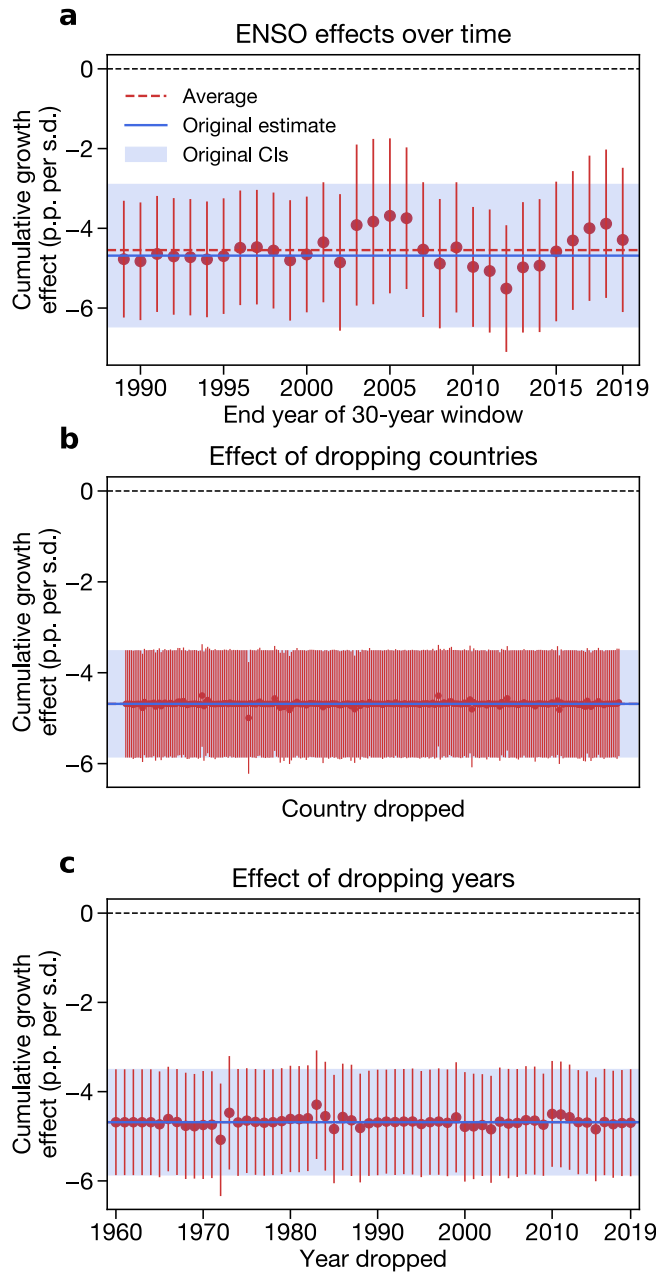
870 model that excludes countries with teleconnection values greater than 0.8 (red dash-dot line), and
871 a model that includes outliers with absolute values of growth greater than 18% (red dashed line).
872 B) Uncertainty in the 5-year cumulative marginal effects of El Niño across each model
873 specification at two representative teleconnection values (0.4 and 1.2). Line styles denote
874 alternative models presented in (A). C) Cumulative marginal effects of El Niño for low-income
875 countries (blue) and high-income countries (red), as defined by World Bank income
876 classifications (Methods). D) Cumulative marginal effects of El Niño for countries experiencing
877 wetting in response to El Niño (positive correlation between the E-index and precipitation, blue)
878 and countries experiencing drying (negative correlation between the E-index and precipitation,
879 red). For each of these samples, we use the original teleconnection value calculated with absolute
880 values in the distributed lag model, but split the sample by the sign of the precipitation
881 teleconnection. In (C) and (D), the original model estimated for all countries is shown in black.
882 E) Cumulative marginal effects of El Niño when using the partial correlation coefficient to
883 measure teleconnections (the main analysis) and when using the regression coefficient instead
884 (red). Inset histograms show the distribution of the two teleconnection metrics. F) Cumulative
885 marginal effects of El Niño when using the full sample (the main analysis, black) and when
886 dropping 1983 and 1998 from the sample (red). In panels (C), (D), (E), and (F), solid line
887 denotes the average and shading denotes 95% confidence intervals from bootstrap resampling by
888 country (Methods).
889
890



891

892 **Fig. S5**

893 Comparison of results using alternative teleconnection metrics. A) Distributions of country-level
 894 teleconnections using monthly temperature correlation coefficients (red), monthly precipitation
 895 correlation coefficients (blue), and their sum (gray). All values are positive since we transform
 896 the correlations to absolute values. B) Cumulative 5-lag effect of ENSO on economic growth
 897 using temperature-only teleconnections (red), precipitation-only teleconnections (blue), and
 898 temperature-plus-precipitation teleconnections (black). C) Relationship between teleconnections
 899 from our main analysis (maximum of three-month running mean) and alternative teleconnections
 900 using the sum of all statistically significant correlation coefficients across the months for each
 901 country. Rho denotes the Spearman's rank correlation coefficient between the two teleconnection
 902 metrics. D) Cumulative 5-lag effect of ENSO on economic growth using the original metric
 903 (black) and the summed correlation coefficient teleconnection metric (red). In (B) and (D), solid
 904 line shows mean and shading shows 95% confidence intervals across 1000 bootstrap iterations,
 905 as in the main analysis.
 906

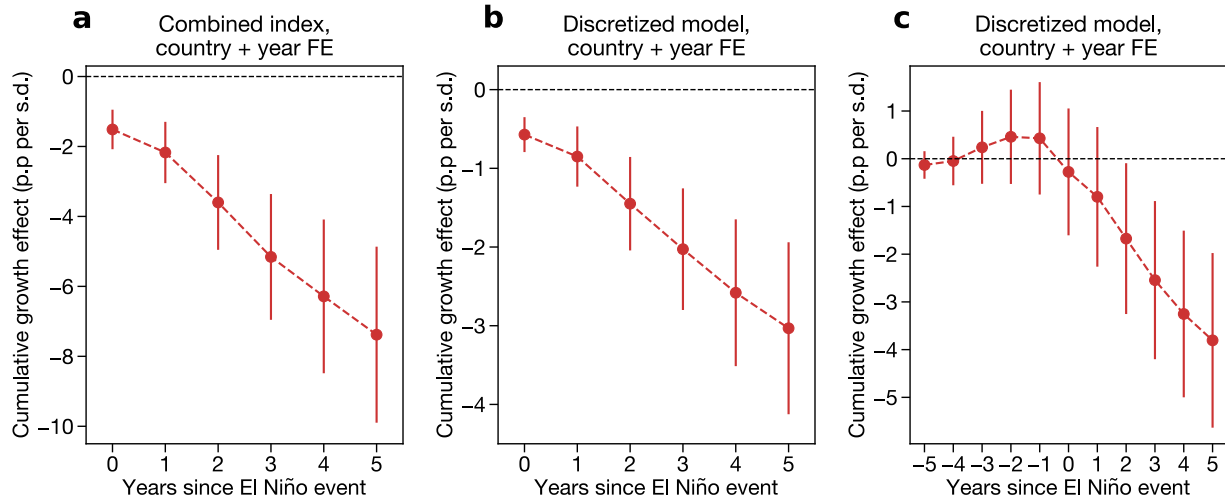


907

908 **Fig. S6**

909 Treatment effect heterogeneity. Panel (A) shows the effect of ENSO on countries with $\tau = 1.0$
 910 calculated in thirty-year rolling windows. X-axis tick refers to the last year of the window. Panel
 911 (B) shows the effect of ENSO on countries with $\tau = 1.0$ when individual countries are dropped
 912 from the sample. We omit country labels for simplicity. Panel (C) shows the effect of ENSO on
 913 countries with $\tau = 1.0$ when individual years are dropped from the sample. In all panels, dashed
 914 red line shows the average effect from all the subsamples, solid blue line shows the central
 915 estimate from our original model, and blue shading shows the 95% confidence interval from our
 916 original model.

917
 918



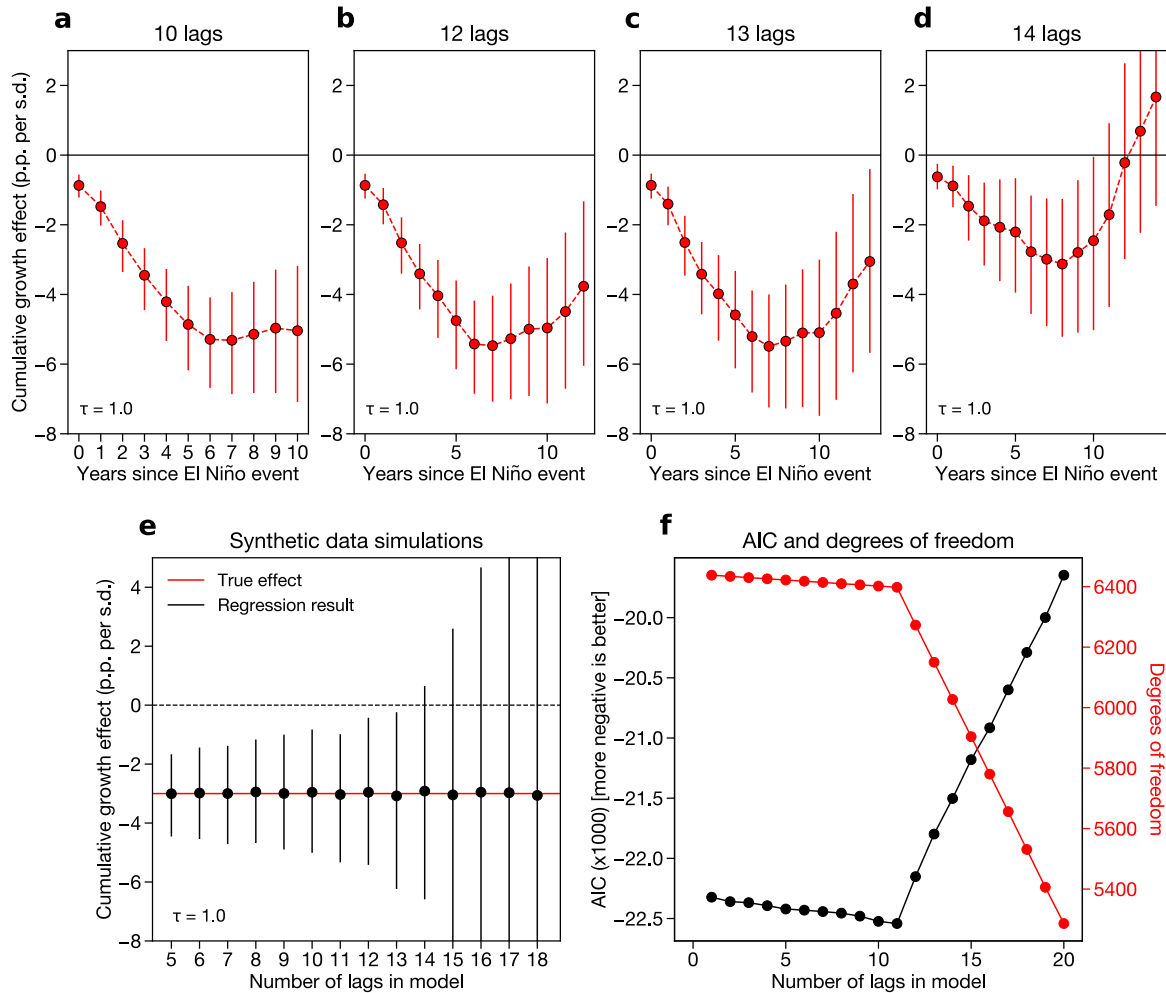
919

920 **Fig. S7**

921 Regression results using several alternative models with both country and year fixed effects.
 922 Panel (A) shows the cumulative effect of a 1-unit increase in the combined index resulting from
 923 multiplying E and τ^E . This index varies in both space and time simultaneously, meaning that both
 924 country and year fixed effects can be included. Panel (B) shows the average cumulative effect of
 925 a 1-s.d. increase in E across all “treated” countries, where treated countries are defined as those
 926 with $\tau^E > 0.5$. Panel (C) shows the same result as (B), with five leads of the E -index added along
 927 with lags. In all cases, the central dashed line shows the mean marginal effect and vertical bars
 928 show the 95% confidence intervals from bootstrap resampling by country.

929

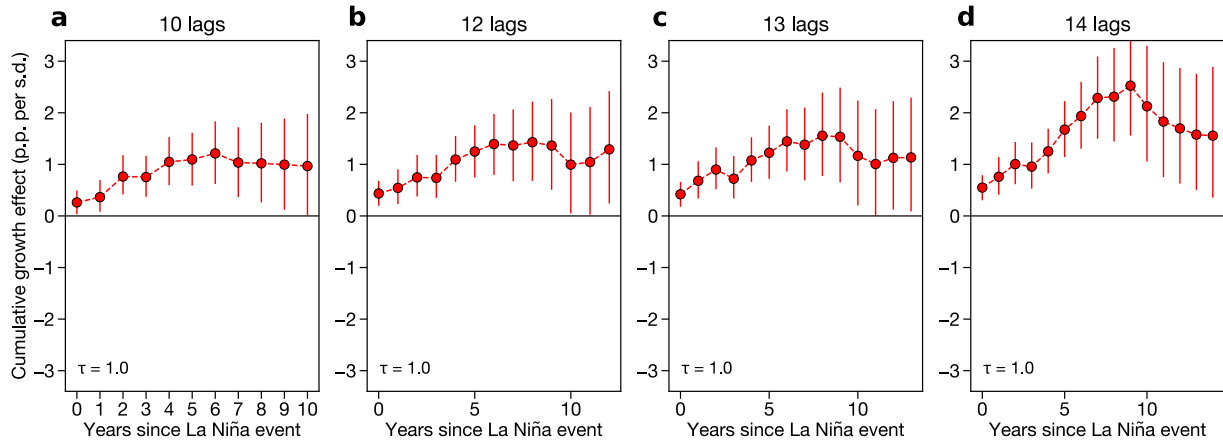
930



931

932 **Fig. S8**

933 Sensitivity of main regression results to additional lags. A-D) Regression results for countries
 934 with teleconnections greater than or equal to 1.0, estimated with 10 (A), 12 (B), 13 (C), or 14 (D)
 935 lags in the regression model. Confidence intervals are estimated by bootstrap resampling as in
 936 the main analysis. E) Results from synthetic data simulations where a “true” negative ENSO
 937 growth effect is imputed to the data and then estimated using models with lags between 5 and 18
 938 (Methods). Coefficients estimated using this perfect model framework are shown for a
 939 hypothetical country with $\tau = 1.0$. F) Black line shows Akaike Information Criterion (AIC)
 940 values for a series of regression models with an increasing number of lags from 1 to 20. More
 941 negative AIC values are more desirable. AIC values are divided by 1000 for readability. Red line
 942 shows the number of degrees of freedom for the same set of models.
 943

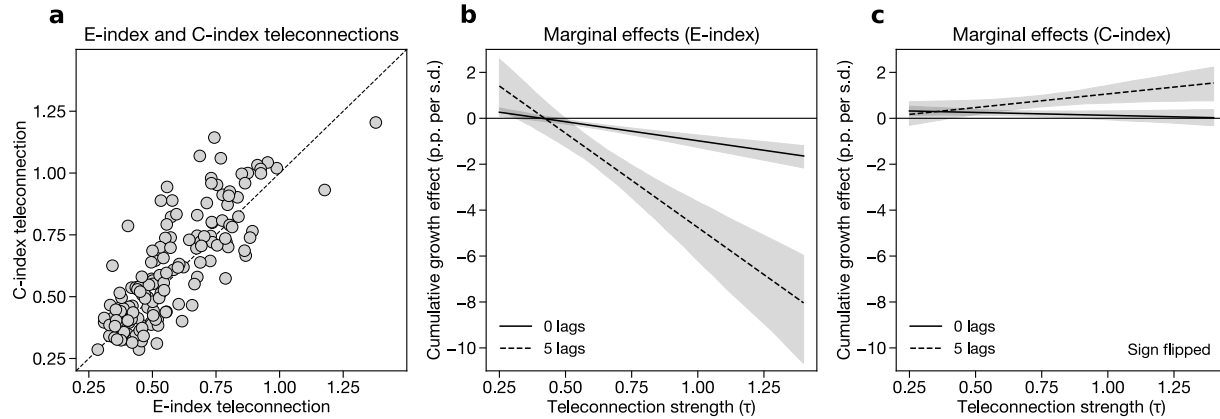


944

945 **Fig. S9**

946 Sensitivity of C-index regression results to additional lags. As in Fig. S7a-d, but for the C-index
 947 coefficients. The sign on the coefficients is flipped to measure the effect of moving from 0 to -1
 948 (i.e., moving a neutral state to a La Niña state).

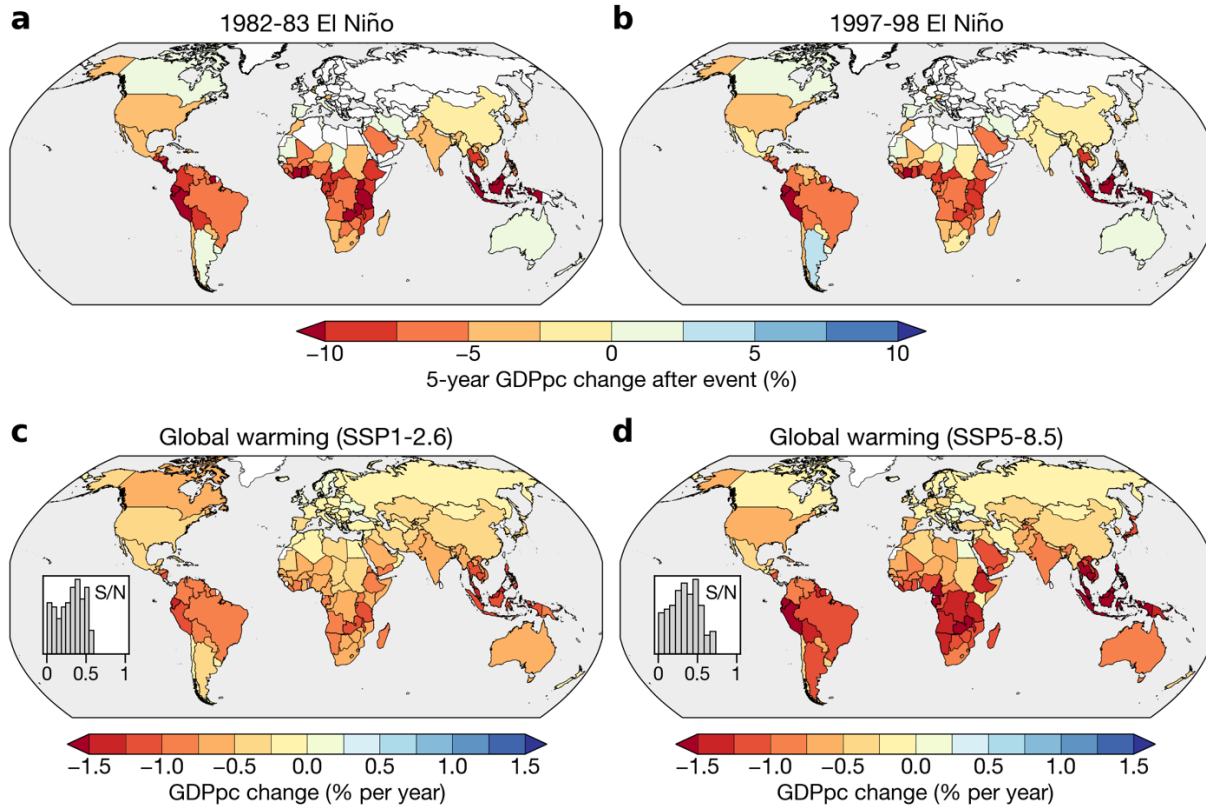
949



950

951 **Fig. S10**

952 Teleconnections and marginal effects for both the E-index and C-index. A) Comparison of
 953 country-specific teleconnection metrics calculated using the E-index (x-axis) and C-index (y-
 954 axis). Dashed line denotes the one-to-one line. B) Marginal effects of El Niño (measured by the
 955 E-index) at 0 and 5 lags across a range of teleconnection values. C) Marginal effects of La Niña
 956 (measured by the C-index) at 0 and 5 lags across a range of teleconnection values. The sign on
 957 the coefficients in (C) is flipped to measure the effect of moving from 0 to -1 (i.e., moving from
 958 a neutral state to a La Niña state). In (B) and (C), effects are calculated from a regression that
 959 includes both the E-index and C-index and their corresponding teleconnection metrics
 960 (Methods). Lines denote averages and shading denotes 95% confidence intervals using bootstrap
 961 resampling by country (Methods).



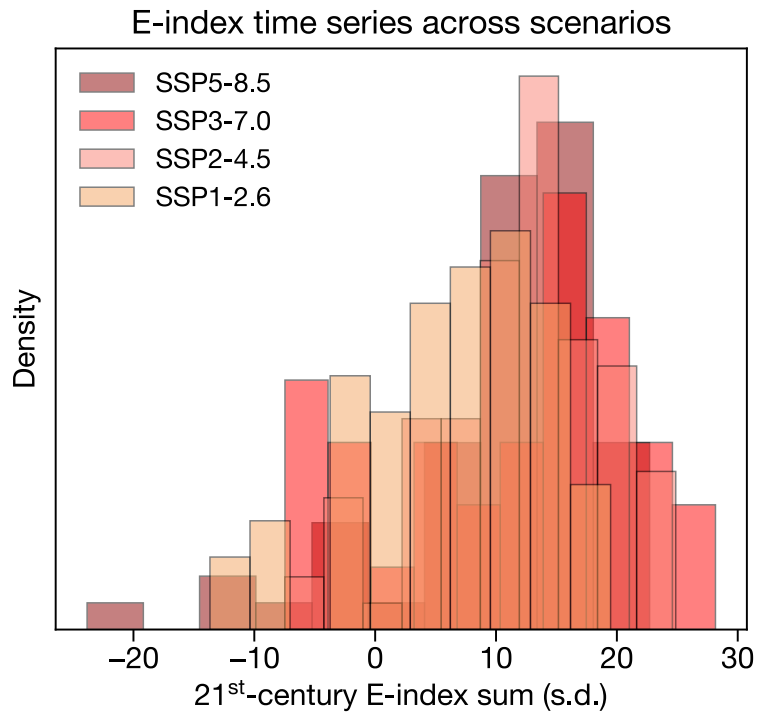
962

963

Fig. S11

964 Country-level losses from extreme El Niño events and global warming. A, B) Change in country-
 965 level GDPpc five years after two specific extreme El Niño events: 1982-83 (A) and 1997-98 (B).
 966 Changes are calculated relative to counterfactual trajectories in which the event did not occur
 967 (see Fig. 2a for example of Peru). That is, the color for Brazil in panel B indicates that Brazil's
 968 GDP per capita would have been 5% larger in 2003 if the 1997-98 El Niño event did not occur.
 969 Countries are masked in white if they either have no significant marginal effect of ENSO or do
 970 not have continuous GDPpc data since 1982 (Methods). C, D) 2020-2099 average change in
 971 country-level GDPpc under the SSP1-2.6 (C) and SSP5-8.5 (D) scenarios for the average case
 972 across climate models and regression bootstraps. Insets in C and D show the signal-to-noise
 973 ratios (S/N), meaning the absolute value of the ratio of the ensemble mean GDPpc change to the
 974 ensemble standard deviation GDPpc change. "Ensemble" is defined as all possible combinations
 975 of climate model projections and regression bootstraps.

976

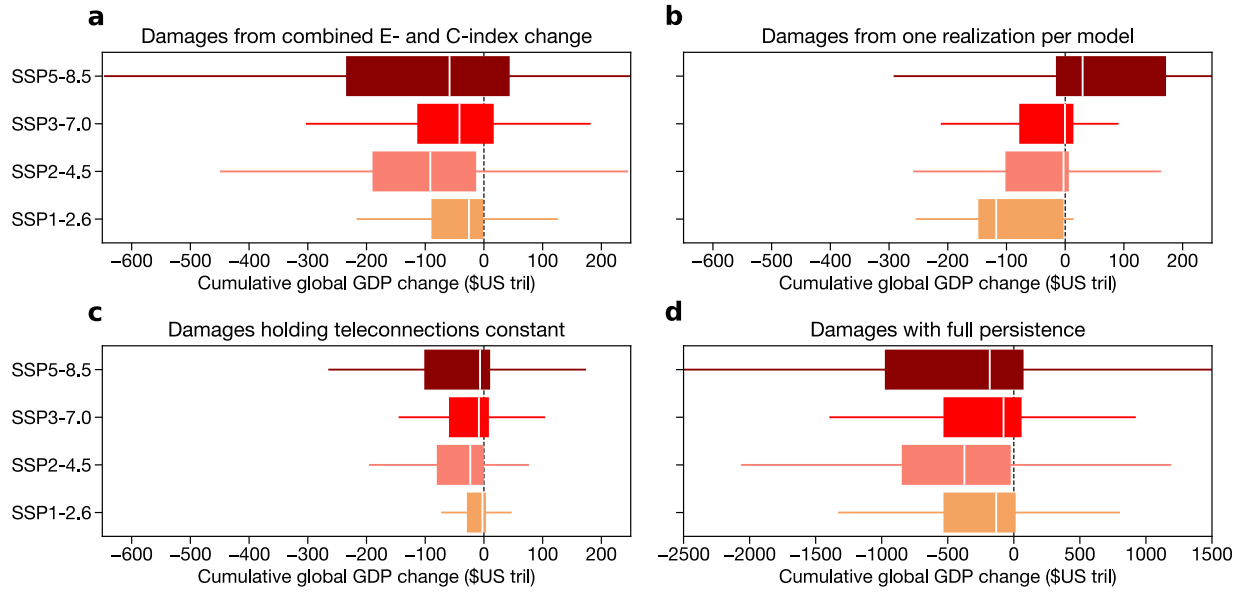


977

978 **Fig. S12**

979 E-index sum across scenarios. Histograms show the distribution of 2020-99 E-index sum values
 980 across simulations within each SSP scenario. Positive values mean that the simulation's E-index
 981 time series has more El Niños than La Niñas.

982



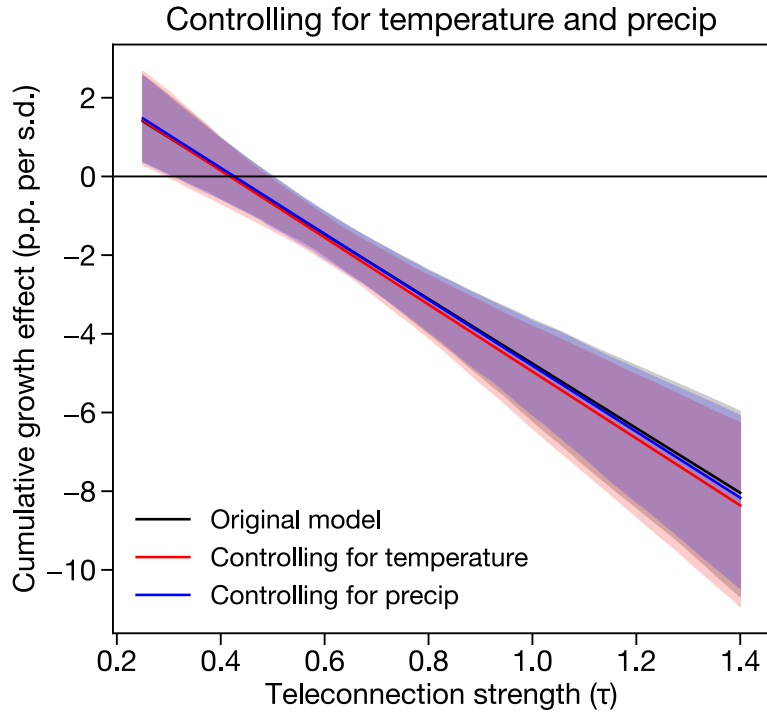
983

984 **Fig. S13**

985 Sensitivity of damage calculations to alternative choices. As in main text Fig. 4a, but for damages due to
 986 the combination of changes in E- and C-index amplitude and teleconnections (A), E-index damages using
 987 only the first realization from each model (B), E-index damages using amplitude change but holding
 988 teleconnections constant (C), and E-index damages when allowing damages to be permanently persistent
 989 (i.e., using the 5-lag model and assuming that the cumulative effects are never recovered) (D). All panels
 990 use a constant 2% discount rate.

991

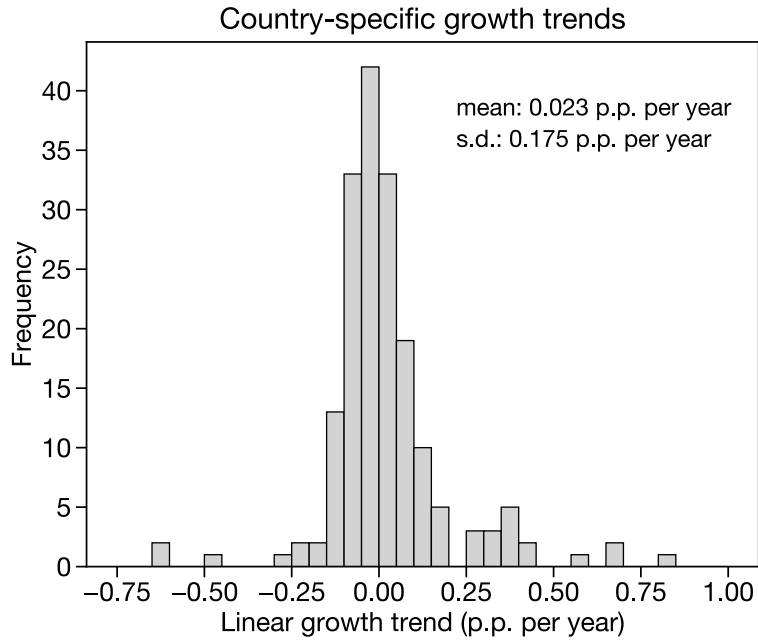
992



993

994 **Fig. S14**

995 Effects of controlling for temperature and precipitation in our regression model. Black line
 996 shows results from the original model, red line shows results with the addition of linear and
 997 quadratic terms for country-level annual mean temperature, and blue line shows results with the
 998 addition of linear and quadratic terms for the country-level annual average of monthly total
 999 precipitation. Shading shows the 95% confidence intervals from bootstrap resampling by
 1000 country, as in the main analysis.
 1001



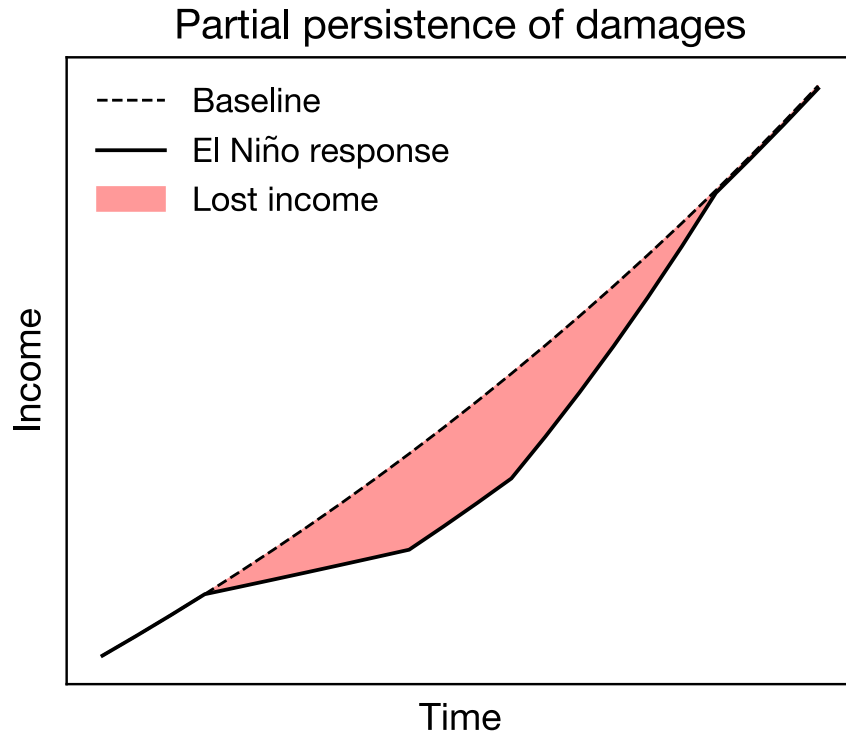
1002

1003 **Fig. S15**

1004 Linear trends in growth. Growth trends are calculated as the linear coefficient on the univariate
 1005 regression of each country's growth time series onto time. Only countries with 10 or more years
 1006 of growth data are included in this histogram. Text in the top right denotes the mean and standard
 1007 deviation of the distribution of trends across countries.

1008

1009



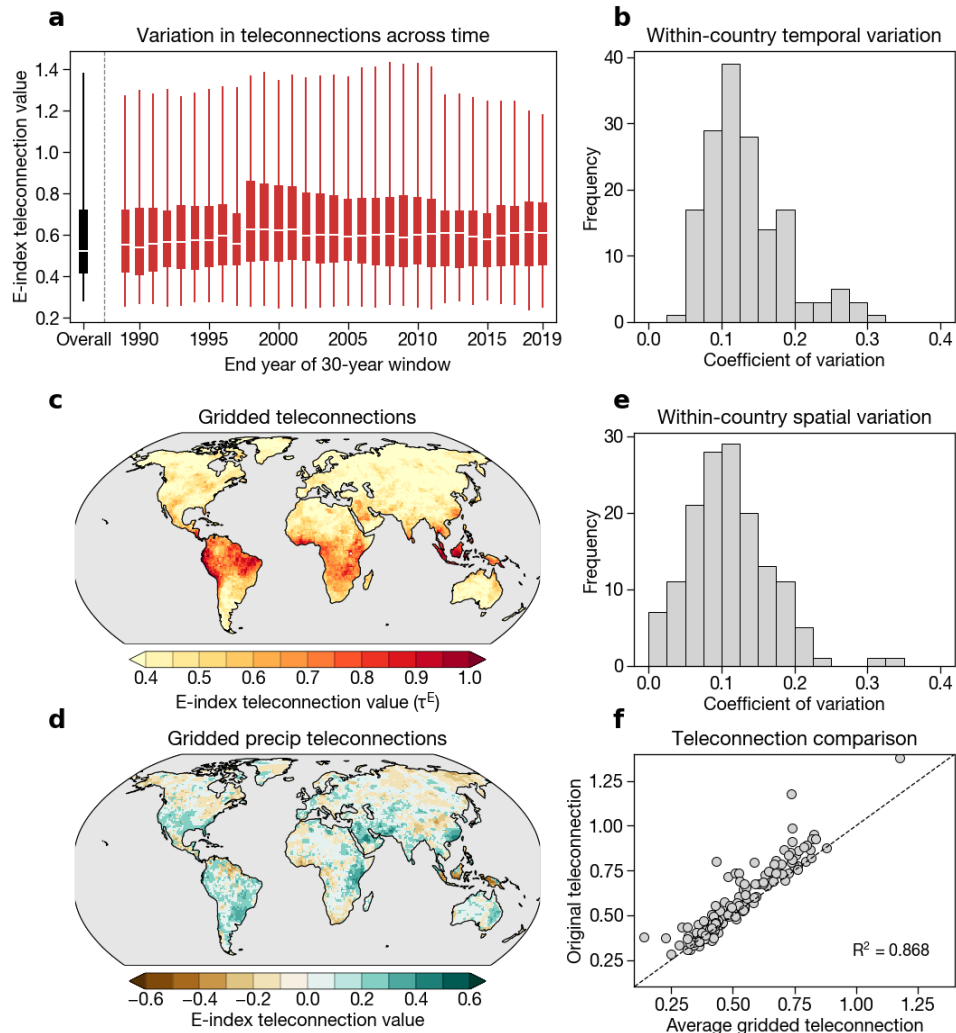
1010

1011 **Fig. S16**

1012 Partial persistence of economic damages. This figure shows a schematic of how we implement
1013 the recovery period in our damage projections. El Niño events negatively affect growth in the
1014 year of the event and in the five years following the event, as in our main model. However, from
1015 years 9 to 14, we allow economies to recover back to their baseline economic trajectory. In the
1016 meantime, there is substantial lost income relative to that baseline trajectory, shown as the red
1017 shaded area.

1018

1019



1020

1021 **Fig. S17**

1022 Spatiotemporal heterogeneity of observed teleconnections. A) Distribution of E-index
 1023 teleconnections in 30-year windows, with x-axis marking the final year of the 30-year window.
 1024 An end year of 2015, for example, implies a start year of 1986. The black boxplot shows the
 1025 original distribution of teleconnections calculated over the whole 1960-2019 period. White lines
 1026 show medians, boxes extend to the 25th and 75th percentiles, and whiskers span the range of the
 1027 data. B) Within-country temporal variation, calculated as the coefficient of variation over the 30-
 1028 year windows shown in (A). This calculation is performed by dividing the standard deviation of
 1029 each country's teleconnection values over all 30-year windows by its mean teleconnection over
 1030 those windows. C) Grid-cell E-index teleconnections, calculated using the same method as the
 1031 country-level teleconnections, but with standardized grid-cell temperature and precipitation data.
 1032 D) Grid-cell precipitation teleconnections, meaning the precipitation component of (C). Note that
 1033 the sign is preserved in (D), whereas the teleconnections in (C) and in the main analysis use
 1034 absolute values. E) Within-country spatial variation in teleconnections, calculated as the
 1035 coefficient of variation of the grid-cell teleconnections when aggregated to the country scale. F)
 1036 Relationship between gridded teleconnections averaged at the country scale (with population
 1037 weighting) and the original teleconnections using country-average temperature and precipitation.
 1038

1039 **Table S1.**
1040 E-index coefficients with alternative clustering techniques. E-index regression coefficients from
1041 the main regression model (Eqn. 1) using various parametric standard error clustering schemes.
1042 The marginal effect of the E-index for a country i is calculated as the main effect of the E-index
1043 plus the interaction term times $\tau_i^E (\beta + \theta * \tau_i^E, \text{Eqn. 2})$. Clustering accounts for both
1044 spatiotemporal autocorrelation in errors as well as heteroskedasticity across clusters. In all
1045 models, the C-index terms and the country fixed effect are included but not shown in the table
1046 for simplicity.
1047

	<i>Dependent variable: growth</i>				
	(1)	(2)	(3)	(4)	(5)
$E_t (\beta_0)$	0.0066*** (0.0016)	0.0066* (0.0033)	0.0066 (0.0035)	0.0066* (0.0025)	0.0066 (0.0041)
$E_{t-1} (\beta_1)$	0.0019 (0.0018)	0.0019 (0.0028)	0.0019 (0.0034)	0.0019 (0.0025)	0.0019 (0.0033)
$E_{t-2} (\beta_2)$	0.0054* (0.0022)	0.0054 (0.0044)	0.0054 (0.0043)	0.0054 (0.0041)	0.0054 (0.0039)
$E_{t-3} (\beta_3)$	0.0081*** (0.0021)	0.0081* (0.0036)	0.0081* (0.0035)	0.0081* (0.0029)	0.0081* (0.0032)
$E_{t-4} (\beta_4)$	0.0053** (0.0019)	0.0053 (0.0033)	0.0053* (0.0026)	0.0053* (0.0020)	0.0053* (0.0023)
$E_{t-5} (\beta_5)$	0.0064** (0.0021)	0.0064* (0.0031)	0.0064* (0.0030)	0.0064** (0.0014)	0.0064* (0.0031)
$E_t \times \tau_i^E (\Theta_0)$	-0.0163*** (0.0028)	-0.0163** (0.0055)	-0.0163*** (0.0042)	-0.0163** (0.0036)	-0.0163*** (0.0051)
$E_{t-1} \times \tau_i^E (\Theta_1)$	-0.0072* (0.0028)	-0.0072 (0.0039)	-0.0072 (0.0043)	-0.0072 (0.0030)	-0.0072 (0.0047)
$E_{t-2} \times \tau_i^E (\Theta_2)$	-0.0158*** (0.0036)	-0.0158** (0.0059)	-0.0158*** (0.0048)	-0.0158* (0.0061)	-0.0158*** (0.0046)
$E_{t-3} \times \tau_i^E (\Theta_3)$	-0.0169*** (0.0032)	-0.0169*** (0.0050)	-0.0169*** (0.0042)	-0.0169** (0.0036)	-0.0169*** (0.0038)
$E_{t-4} \times \tau_i^E (\Theta_4)$	-0.0123*** (0.0032)	-0.0123** (0.0045)	-0.0123*** (0.0029)	-0.0123** (0.0024)	-0.0123*** (0.0025)
$E_{t-5} \times \tau_i^E (\Theta_5)$	-0.0121*** (0.0034)	-0.0121* (0.0048)	-0.0121*** (0.0035)	-0.0121*** (0.0010)	-0.0121*** (0.0035)
Observations	7183	7183	7183	7183	7183
Clustering	Country	Year-continent	Year	Continent	Five-year block

*** $p < 0.001$; ** $p < 0.01$; * $p < 0.05$

1048

1049 **Table S2.**
1050 C-index coefficients with alternative clustering techniques. C-index regression coefficients from
1051 the main regression model (Eqn. 1) using various parametric standard error clustering schemes.
1052 The marginal effect of the C-index for a country i is calculated as the main effect of the C-index
1053 plus the interaction term times τ_i^C ($\phi + \Psi * \tau_i^C$, Eqn. 2). Clustering accounts for both
1054 spatiotemporal autocorrelation in errors as well as heteroskedasticity across clusters. In all
1055 models, the E-index terms and the country fixed effect are included but not shown in the table for
1056 simplicity.
1057

	<i>Dependent variable: growth</i>				
	(1)	(2)	(3)	(4)	(5)
$C_t (\Phi_0)$	-0.0038* (0.0016)	-0.0038 (0.0028)	-0.0038 (0.0032)	-0.0038 (0.0015)	-0.0038 (0.0052)
$C_{t-1} (\Phi_1)$	0.0048*** (0.0013)	0.0048 (0.0043)	0.0048 (0.0044)	0.0048 (0.0020)	0.0048 (0.0041)
$C_{t-2} (\Phi_2)$	0.0021 (0.0012)	0.0021 (0.0036)	0.0021 (0.0042)	0.0021 (0.0009)	0.0021 (0.0021)
$C_{t-3} (\Phi_3)$	0.0028** (0.0010)	0.0028 (0.0033)	0.0028 (0.0039)	0.0028 (0.0014)	0.0028 (0.0027)
$C_{t-4} (\Phi_4)$	-0.0015 (0.0013)	-0.0015 (0.0035)	-0.0015 (0.0040)	-0.0015 (0.0011)	-0.0015 (0.0021)
$C_{t-5} (\Phi_5)$	-0.0031* (0.0015)	-0.0031 (0.0026)	-0.0031 (0.0032)	-0.0031*** (0.0004)	-0.0031 (0.0042)
$C_t \times \tau_i^C (\Psi_0)$	0.0026 (0.0023)	0.0026 (0.0039)	0.0026 (0.0042)	0.0026 (0.0017)	0.0026 (0.0067)
$C_{t-1} \times \tau_i^C (\Psi_1)$	-0.0074*** (0.0018)	-0.0074 (0.0056)	-0.0074 (0.0051)	-0.0074 (0.0031)	-0.0074 (0.0047)
$C_{t-2} \times \tau_i^C (\Psi_2)$	-0.0059** (0.0018)	-0.0059 (0.0047)	-0.0059 (0.0048)	-0.0059** (0.0011)	-0.0059* (0.0026)
$C_{t-3} \times \tau_i^C (\Psi_3)$	-0.0041** (0.0015)	-0.0041 (0.0044)	-0.0041 (0.0046)	-0.0041* (0.0013)	-0.0041 (0.0034)
$C_{t-4} \times \tau_i^C (\Psi_4)$	0.0005 (0.0019)	0.0005 (0.0047)	0.0005 (0.0046)	0.0005 (0.0012)	0.0005 (0.0028)
$C_{t-5} \times \tau_i^C (\Psi_5)$	0.0025 (0.0020)	0.0025 (0.0035)	0.0025 (0.0034)	0.0025* (0.0007)	0.0025 (0.0045)
Observations	7183	7183	7183	7183	7183
Clustering	Country	Year-continent	Year	Continent	Five-year block

*** $p < 0.001$; ** $p < 0.01$; * $p < 0.05$

1058
1059

1060 **Table S3.**
 1061 CMIP6 models and realizations used from the SSP1-2.6 scenario. Monthly sea surface
 1062 temperature (“tos”), monthly atmospheric temperature (“tas”), and daily precipitation (“pr”) are
 1063 used from each model. Bolded models are those that have at least 1 realization selected for the
 1064 final analysis (Methods).
 1065

Model	Total realizations	Selected realizations
CanESM5	50	0
KACE-1-0-G	3	0
MIROC-ES2L	7	7
MIROC6	50	50
MRI-ESM2-0	5	4

1066
 1067

1068 **Table S4.**
 1069 CMIP6 models and realizations used from the SSP2-4.5 scenario. Monthly sea surface
 1070 temperature (“tos”), monthly atmospheric temperature (“tas”), and daily precipitation (“pr”) are
 1071 used from each model. Bolded models are those that have at least 1 realization selected for the
 1072 final analysis (Methods).
 1073

Model	Total realizations	Selected realizations
ACCESS-CM2	3	0
ACCESS-ESM1-5	11	0
CAMS-CSM1-0	1	0
CESM2	2	0
CESM2-WACCM	3	2
CMCC-CM2-SR5	1	1
CMCC-ESM2	1	1
CNRM-CM6-1	1	0
CanESM5	50	0
EC-Earth3	8	8
FGOALS-g3	3	0
GFDL-ESM4	1	0
HadGEM3-GC31-LL	1	0
INM-CM4-8	1	0
INM-CM5-0	1	0
IPSL-CM6A-LR	5	0
KACE-1-0-G	3	0
MIROC-ES2L	30	30
MIROC6	33	33
MPI-ESM1-2-HR	2	1
MPI-ESM1-2-LR	10	9
NorESM2-LM	2	0
NorESM2-MM	2	1
UKESM1-0-LL	5	0

1074
 1075
 1076

1077 **Table S5.**
 1078 CMIP6 models and realizations used from the SSP3-7.0 scenario. Monthly sea surface
 1079 temperature (“tos”), monthly atmospheric temperature (“tas”), and daily precipitation (“pr”) are
 1080 used from each model. Bolded models are those that have at least 1 realization selected for the
 1081 final analysis (Methods).
 1082

Model	Total realizations	Selected realizations
ACCESS-CM2	3	0
ACCESS-ESM1-5	10	0
CAMS-CSM1-0	1	0
CESM2	2	0
CESM2-WACCM	1	1
CMCC-CM2-SR5	1	1
CMCC-ESM2	1	1
CNRM-CM6-1	1	0
CanESM5	50	0
FGOALS-g3	4	0
GFDL-ESM4	1	0
INM-CM4-8	1	0
INM-CM5-0	5	0
IPSL-CM6A-LR	5	0
KACE-1-0-G	3	0
MIROC-ES2L	10	10
MIROC6	3	3
MPI-ESM1-2-HR	10	4
MPI-ESM1-2-LR	7	6
MRI-ESM2-0	5	5
NorESM2-LM	1	1
NorESM2-MM	1	1
UKESM1-0-LL	13	0

1083
 1084
 1085

1086 **Table S6.**
 1087 CMIP6 models and realizations used from the SSP5-8.5 scenario. Monthly sea surface
 1088 temperature (“tos”), monthly atmospheric temperature (“tas”), and daily precipitation (“pr”) are
 1089 used from each model. Bolded models are those that have at least 1 realization selected for the
 1090 final analysis (Methods).
 1091

Model	Total realizations	Selected realizations
ACCESS-CM2	2	0
ACCESS-ESM1-5	6	0
CAMS-CSM1-0	1	0
CESM2	0	0
CESM2-WACCM	3	1
CMCC-CM2-SR5	1	1
CMCC-ESM2	1	1
CNRM-CM6-1	1	0
CanESM5	50	0
FGOALS-g3	3	0
GFDL-ESM4	1	0
HadGEM3-GC31-LL	4	0
HadGEM3-GC31-MM	4	0
INM-CM4-8	1	0
INM-CM5-0	1	0
IPSL-CM6A-LR	4	0
KACE-1-0-G	3	0
MIROC-ES2L	1	1
MIROC6	50	50
MPI-ESM1-2-HR	2	1
NorESM2-LM	1	1
NorESM2-MM	1	1
UKESM1-0-LL	5	0

1092
 1093

1094 **Table S7.**
 1095 Correlation matrix for the E-index and its lags. Each table entry shows the Pearson correlation
 1096 coefficient between the E-index at various time lags and the E-index at each other time lag.
 1097

	E_t	E_{t-1}	E_{t-2}	E_{t-3}	E_{t-4}	E_{t-5}
E_t		-0.101	-0.335	0.002	0.034	0.002
E_{t-1}			-0.092	-0.336	-0.01	0.037
E_{t-2}				-0.089	-0.291	-0.029
E_{t-3}					-0.094	-0.291
E_{t-4}						-0.076

1098

1099 **References and Notes**

- 1100 1. M. J. McPhaden, S. E. Zebiak, M. H. Glantz, ENSO as an Integrating Concept in Earth Science.
1101 *Science*. **314**, 1740–1745 (2006).
- 1102 2. J. Bjerknes, ATMOSPHERIC TELECONNECTIONS FROM THE EQUATORIAL PACIFIC. *Mon.*
1103 *Weather Rev.* **97**, 163–172 (1969).
- 1104 3. S.-W. Yeh, W. Cai, S.-K. Min, M. J. McPhaden, D. Dommenges, B. Dewitte, M. Collins, K. Ashok,
1105 S.-I. An, B.-Y. Yim, J.-S. Kug, ENSO Atmospheric Teleconnections and Their Response to
1106 Greenhouse Gas Forcing. *Rev. Geophys.* **56**, 185–206 (2018).
- 1107 4. T. W. Corringham, D. R. Cayan, The Effect of El Niño on Flood Damages in the Western United
1108 States. *Weather Clim. Soc.* **11**, 489–504 (2019).
- 1109 5. F. J. Magilligan, P. S. Goldstein, El Niño floods and culture change: A late Holocene flood history
1110 for the Rio Moquegua, southern Peru. *Geology*. **29**, 431–434 (2001).
- 1111 6. S. M. Hsiang, K. C. Meng, Tropical Economics. *Am. Econ. Rev.* **105**, 257–261 (2015).
- 1112 7. T. Iizumi, J.-J. Luo, A. J. Challinor, G. Sakurai, M. Yokozawa, H. Sakuma, M. E. Brown, T.
1113 Yamagata, Impacts of El Niño Southern Oscillation on the global yields of major crops. *Nat.*
1114 *Commun.* **5**, 3712 (2014).
- 1115 8. S. M. Hsiang, K. C. Meng, M. A. Cane, Civil conflicts are associated with the global climate. *Nature*.
1116 **476**, 438–441 (2011).
- 1117 9. W. Cai, G. Wang, B. Dewitte, L. Wu, A. Santoso, K. Takahashi, Y. Yang, A. Carréric, M. J.
1118 McPhaden, Increased variability of eastern Pacific El Niño under greenhouse warming. *Nature*. **564**,
1119 201–206 (2018).
- 1120 10. W. Cai, B. Ng, G. Wang, A. Santoso, L. Wu, K. Yang, Increased ENSO sea surface temperature
1121 variability under four IPCC emission scenarios. *Nat. Clim. Change*, 1–4 (2022).
- 1122 11. W. Cai, S. Borlace, M. Lengaigne, P. van Rensch, M. Collins, G. Vecchi, A. Timmermann, A.
1123 Santoso, M. J. McPhaden, L. Wu, M. H. England, G. Wang, E. Guilyardi, F.-F. Jin, Increasing
1124 frequency of extreme El Niño events due to greenhouse warming. *Nat. Clim. Change*. **4**, 111–116
1125 (2014).
- 1126 12. W. Cai, A. Santoso, M. Collins, B. Dewitte, C. Karamperidou, J.-S. Kug, M. Lengaigne, M. J.
1127 McPhaden, M. F. Stuecker, A. S. Taschetto, A. Timmermann, L. Wu, S.-W. Yeh, G. Wang, B. Ng,
1128 F. Jia, Y. Yang, J. Ying, X.-T. Zheng, T. Bayr, J. R. Brown, A. Capotondi, K. M. Cobb, B. Gan, T.
1129 Geng, Y.-G. Ham, F.-F. Jin, H.-S. Jo, X. Li, X. Lin, S. McGregor, J.-H. Park, K. Stein, K. Yang, L.
1130 Zhang, W. Zhong, Changing El Niño–Southern Oscillation in a warming climate. *Nat. Rev. Earth*
1131 *Environ.* **2**, 628–644 (2021).
- 1132 13. M. Burke, S. M. Hsiang, E. Miguel, Global non-linear effect of temperature on economic production.
1133 *Nature*. **527**, 235–239 (2015).
- 1134 14. M. Burke, V. Tanutama, Climatic constraints on aggregate economic output. *Natl. Bur. Econ. Res.*
1135 *Work. Pap.* (2019).

- 1136 15. M. Dell, B. F. Jones, B. A. Olken, Temperature shocks and economic growth: Evidence from the last
1137 half century. *Am. Econ. J. Macroecon.* **4**, 66–95 (2012).
- 1138 16. M. Kalkuhl, L. Wenz, The impact of climate conditions on economic production. Evidence from a
1139 global panel of regions. *J. Environ. Econ. Manag.* **103**, 102360 (2020).
- 1140 17. M. Kotz, L. Wenz, A. Stechemesser, M. Kalkuhl, A. Levermann, Day-to-day temperature variability
1141 reduces economic growth. *Nat. Clim. Change*, 1–7 (2021).
- 1142 18. P. Cashin, K. Mohaddes, M. Raissi, Fair weather or foul? The macroeconomic effects of El Niño. *J.*
1143 *Int. Econ.* **106**, 37–54 (2017).
- 1144 19. S. C. Smith, D. Ubilava, The El Niño Southern Oscillation and Economic Growth in the Developing
1145 World. *Glob. Environ. Change.* **45**, 151–164 (2017).
- 1146 20. R. Generoso, C. Couharde, O. Damette, K. Mohaddes, The Growth Effects of El Niño and La Niña:
1147 Local Weather Conditions Matter. *Ann. Econ. Stat.*, 83–126 (2020).
- 1148 21. A. D. Brunner, El Niño and World Primary Commodity Prices: Warm Water or Hot Air? *Rev. Econ.*
1149 *Stat.* **84**, 176–183 (2002).
- 1150 22. D. Ubilava, El Niño, La Niña, and world coffee price dynamics. *Agric. Econ.* **43**, 17–26 (2012).
- 1151 23. D. Ubilava, The ENSO Effect and Asymmetries in Wheat Price Dynamics. *World Dev.* **96**, 490–502
1152 (2017).
- 1153 24. F. C. Moore, D. B. Diaz, Temperature impacts on economic growth warrant stringent mitigation
1154 policy. *Nat. Clim. Change.* **5**, 127 (2015).
- 1155 25. S. Dietz, N. Stern, Endogenous growth, convexity of damage and climate risk: how Nordhaus’
1156 framework supports deep cuts in carbon emissions. *Econ. J.* **125**, 574–620 (2015).
- 1157 26. E. J. Moyer, M. D. Woolley, N. J. Matteson, M. J. Glotter, D. A. Weisbach, Climate impacts on
1158 economic growth as drivers of uncertainty in the social cost of carbon. *J. Leg. Stud.* **43**, 401–425
1159 (2014).
- 1160 27. K. Takahashi, A. Montecinos, K. Goubanova, B. Dewitte, ENSO regimes: Reinterpreting the
1161 canonical and Modoki El Niño. *Geophys. Res. Lett.* **38** (2011).
- 1162 28. E. M. Rasmusson, T. H. Carpenter, Variations in Tropical Sea Surface Temperature and Surface
1163 Wind Fields Associated with the Southern Oscillation/El Niño. *Mon. Weather Rev.* **110**, 354–384
1164 (1982).
- 1165 29. D. Ubilava, M. Abdolrahimi, The El Niño impact on maize yields is amplified in lower income
1166 teleconnected countries. *Environ. Res. Lett.* **14**, 054008 (2019).
- 1167 30. S. Power, M. Haylock, R. Colman, X. Wang, The Predictability of Interdecadal Changes in ENSO
1168 Activity and ENSO Teleconnections. *J. Clim.* **19**, 4755–4771 (2006).
- 1169 31. B. A. Bastien-Olvera, F. Granella, F. C. Moore, Persistent effect of temperature on GDP identified
1170 from lower frequency temperature variability. *Environ. Res. Lett.* **17**, 084038 (2022).

- 1171 32. M. Kotz, A. Levermann, L. Wenz, The effect of rainfall changes on economic production. *Nature*.
1172 **601**, 223–227 (2022).
- 1173 33. N. S. Diffenbaugh, F. V. Davenport, M. Burke, Historical warming has increased U.S. crop insurance
1174 losses. *Environ. Res. Lett.* **16**, 084025 (2021).
- 1175 34. W. Cai, G. Wang, A. Santoso, M. J. McPhaden, L. Wu, F.-F. Jin, A. Timmermann, M. Collins, G.
1176 Vecchi, M. Lengaigne, M. H. England, D. Dommenges, K. Takahashi, E. Guilyardi, Increased
1177 frequency of extreme La Niña events under greenhouse warming. *Nat. Clim. Change*. **5**, 132–137
1178 (2015).
- 1179 35. van Aalst, M.K., Fankhauser, S., Kane, S.M., Sponberg, K., Climate information and forecasting for
1180 development: lessons from the 1997/98 El Niño (2000).
- 1181 36. W. Cai, B. Ng, T. Geng, L. Wu, A. Santoso, M. J. McPhaden, Butterfly effect and a self-modulating
1182 El Niño response to global warming. *Nature*. **585**, 68–73 (2020).
- 1183 37. N. Maher, D. Matei, S. Milinski, J. Marotzke, ENSO change in climate projections: forced response
1184 or internal variability? *Geophys. Res. Lett.* **45**, 11–390 (2018).
- 1185 38. C. Deser, R. Knutti, S. Solomon, A. S. Phillips, Communication of the role of natural variability in
1186 future North American climate. *Nat. Clim. Change*. **2**, 775–779 (2012).
- 1187 39. K.-S. Yun, J.-Y. Lee, A. Timmermann, K. Stein, M. F. Stuecker, J. C. Fyfe, E.-S. Chung, Increasing
1188 ENSO–rainfall variability due to changes in future tropical temperature–rainfall relationship.
1189 *Commun. Earth Environ.* **2**, 1–7 (2021).
- 1190 40. K. Hu, G. Huang, P. Huang, Y. Kosaka, S.-P. Xie, Intensification of El Niño-induced atmospheric
1191 anomalies under greenhouse warming. *Nat. Geosci.* **14**, 377–382 (2021).
- 1192 41. A. T. Wittenberg, A. Rosati, T. L. Delworth, G. A. Vecchi, F. Zeng, ENSO Modulation: Is It
1193 Decadally Predictable? *J. Clim.* **27**, 2667–2681 (2014).
- 1194 42. C. W. Callahan, C. Chen, M. Rugenstein, J. Bloch-Johnson, S. Yang, E. J. Moyer, Robust decrease in
1195 El Niño/Southern Oscillation amplitude under long-term warming. *Nat. Clim. Change*. **11**, 752–757
1196 (2021).
- 1197 43. Council of Economic Advisers, Discounting for public policy: Theory and recent evidence on the
1198 merits of updating the discount rate (2017), (available at
1199 https://obamawhitehouse.archives.gov/sites/default/files/page/files/201701_cea_discounting_issue_brief.pdf).
1200
- 1201 44. M. Meinshausen, J. Lewis, C. McGlade, J. Gütschow, Z. Nicholls, R. Burdon, L. Cozzi, B.
1202 Hackmann, Realization of Paris Agreement pledges may limit warming just below 2 °C. *Nature*.
1203 **604**, 304–309 (2022).
- 1204 45. M. Davis, *Late Victorian Holocausts: El Niño Famines and the Making of the Third World* (Verso
1205 Books, 2002).
- 1206 46. C. W. Callahan, J. S. Mankin, Globally unequal effect of extreme heat on economic growth. *Sci. Adv.*
1207 **8**, eadd3726 (2022).

- 1208 47. B. O'Neill, M. van Aalst, Z. Zaiton Ibrahim, L. Berrang Ford, S. Bhadwal, H. Buhaug, D. Diaz, K.
1209 Frieler, M. Garschagen, A. Magnan, G. Midgely, A. Mirzabaev, A. Thomas, R. Warren, "Key Risks
1210 Across Sectors and Regions" in *Climate Change 2022: Impacts, Adaptation and Vulnerability.*
1211 *Contribution of Working Group II to the Sixth Assessment Report of the Intergovernmental Panel on*
1212 *Climate Change* (Cambridge University Press, Cambridge, UK and New York, NY, USA, 2022),
1213 pp. 2411–2538.
- 1214 48. A. French, R. Mechler, "Managing El Niño risks under uncertainty in Peru" (International Institute
1215 for Applied Systems Analysis, 2017), (available at
1216 [https://pure.iiasa.ac.at/id/eprint/14849/1/French_Mechler_2017_El%20Ni%c3%b1o_Risk_Peru_Re](https://pure.iiasa.ac.at/id/eprint/14849/1/French_Mechler_2017_El%20Ni%c3%b1o_Risk_Peru_Report.pdf)
1217 [port.pdf](https://pure.iiasa.ac.at/id/eprint/14849/1/French_Mechler_2017_El%20Ni%c3%b1o_Risk_Peru_Report.pdf)).
- 1218 49. N. A. Rayner, D. E. Parker, E. B. Horton, C. K. Folland, L. V. Alexander, D. P. Rowell, E. C. Kent,
1219 A. Kaplan, Global analyses of sea surface temperature, sea ice, and night marine air temperature
1220 since the late nineteenth century. *J. Geophys. Res. Atmospheres*. **108** (2003),
1221 doi:10.1029/2002JD002670.
- 1222 50. R. A. Rohde, Z. Hausfather, The Berkeley Earth Land/Ocean Temperature Record. *Earth Syst. Sci.*
1223 *Data Discuss.*, 1–16 (2020).
- 1224 51. U. Schneider, A. Becker, P. Finger, A. Meyer-Christoffer, B. Rudolf, M. Ziese, GPCP full data
1225 reanalysis version 6.0 at 0.5: monthly land-surface precipitation from rain-gauges built on GTS-
1226 based and historic data. *GPCC Data Rep Doi*. **10** (2011).
- 1227 52. C. U. Center for International Earth Science Information Network CIESIN, *Gridded Population of*
1228 *the World, Version 4 (GPWv4): Population Count* (2016).
- 1229 53. R. C. Feenstra, R. Inklaar, M. P. Timmer, The next generation of the Penn World Table. *Am. Econ.*
1230 *Rev.* **105**, 3150–82 (2015).
- 1231 54. A. Deaton, A. Heston, Understanding PPPs and PPP-Based National Accounts. *Am. Econ. J.*
1232 *Macroecon.* **2**, 1–35 (2010).
- 1233 55. T. W. Bank, *World Development Indicators 2016* (2016).
- 1234 56. V. Eyring, S. Bony, G. A. Meehl, C. A. Senior, B. Stevens, R. J. Stouffer, K. E. Taylor, Overview of
1235 the Coupled Model Intercomparison Project Phase 6 (CMIP6) experimental design and
1236 organization. *Geosci. Model Dev.* **9**, 1937–1958 (2016).
- 1237 57. B. C. O'Neill, C. Tebaldi, D. P. van Vuuren, V. Eyring, P. Friedlingstein, G. Hurtt, R. Knutti, E.
1238 Kriegler, J.-F. Lamarque, J. Lowe, G. A. Meehl, R. Moss, K. Riahi, B. M. Sanderson, The Scenario
1239 Model Intercomparison Project (ScenarioMIP) for CMIP6. *Geosci. Model Dev.* **9**, 3461–3482
1240 (2016).
- 1241 58. C. Tebaldi, K. Debeire, V. Eyring, E. Fischer, J. Fyfe, P. Friedlingstein, R. Knutti, J. Lowe, B.
1242 O'Neill, B. Sanderson, D. van Vuuren, K. Riahi, M. Meinshausen, Z. Nicholls, K. B. Tokarska, G.
1243 Hurtt, E. Kriegler, J.-F. Lamarque, G. Meehl, R. Moss, S. E. Bauer, O. Boucher, V. Brovkin, Y.-H.
1244 Byun, M. Dix, S. Gualdi, H. Guo, J. G. John, S. Kharin, Y. Kim, T. Koshiro, L. Ma, D. Olivié, S.
1245 Panickal, F. Qiao, X. Rong, N. Rosenbloom, M. Schupfner, R. Séférian, A. Sellar, T. Semmler, X.
1246 Shi, Z. Song, C. Steger, R. Stouffer, N. Swart, K. Tachiiri, Q. Tang, H. Tatebe, A. Voldoire, E.

- 1247 Volodin, K. Wyser, X. Xin, S. Yang, Y. Yu, T. Ziehn, Climate model projections from the Scenario
1248 Model Intercomparison Project (ScenarioMIP) of CMIP6. *Earth Syst. Dyn.* **12**, 253–293 (2021).
- 1249 59. S. Hoyer, J. Hamman, xarray: N-D labeled arrays and datasets in Python. *J Open Res Softw. Revis.*
1250 (2017).
- 1251 60. F. Jia, W. Cai, B. Gan, L. Wu, E. Di Lorenzo, Enhanced North Pacific impact on El Niño/Southern
1252 Oscillation under greenhouse warming. *Nat. Clim. Change*, 1–8 (2021).
- 1253 61. B. Ng, W. Cai, T. Cowan, D. Bi, Impacts of Low-Frequency Internal Climate Variability and
1254 Greenhouse Warming on El Niño–Southern Oscillation. *J. Clim.* **34**, 2205–2218 (2021).
- 1255 62. E. Tziperman, M. A. Cane, S. E. Zebiak, Y. Xue, B. Blumenthal, Locking of El Niño’s Peak Time to
1256 the End of the Calendar Year in the Delayed Oscillator Picture of ENSO. *J. Clim.* **11**, 2191–2199
1257 (1998).
- 1258 63. M. Newman, P. D. Sardeshmukh, Are we near the predictability limit of tropical Indo-Pacific sea
1259 surface temperatures? *Geophys. Res. Lett.* **44**, 8520–8529 (2017).
- 1260 64. C. D. Kolstad, F. C. Moore, Estimating the economic impacts of climate change using weather
1261 observations. *Rev. Environ. Econ. Policy.* **14**, 1–24 (2020).
- 1262 65. M. Burke, W. M. Davis, N. S. Diffenbaugh, Large potential reduction in economic damages under
1263 UN mitigation targets. *Nature.* **557** (2018).
- 1264 66. S. M. Hsiang, A. S. Jina, The causal effect of environmental catastrophe on long-run economic
1265 growth: Evidence from 6,700 cyclones. *Natl. Bur. Econ. Res. Work. Pap.* (2014).
- 1266 67. S. Hsiang, Climate econometrics. *Annu. Rev. Resour. Econ.* **8**, 43–75 (2016).
- 1267 68. J. H. Stock, M. W. Watson, Vector Autoregressions. *J. Econ. Perspect.* **15**, 101–115 (2001).
- 1268 69. N. S. Diffenbaugh, M. Burke, Global warming has increased global economic inequality. *Proc. Natl.*
1269 *Acad. Sci.* **116**, 9808–9813 (2019).
- 1270 70. E. Guilyardi, A. Wittenberg, A. Fedorov, M. Collins, C. Wang, A. Capotondi, G. J. van Oldenborgh,
1271 T. Stockdale, Understanding El Niño in Ocean–Atmosphere General Circulation Models: Progress
1272 and Challenges. *Bull. Am. Meteorol. Soc.* **90**, 325–340 (2009).
- 1273 71. R. Seager, M. Cane, N. Henderson, D.-E. Lee, R. Abernathey, H. Zhang, Strengthening tropical
1274 Pacific zonal sea surface temperature gradient consistent with rising greenhouse gases. *Nat. Clim.*
1275 *Change.* **9**, 517–522 (2019).
- 1276 72. C. Karamperidou, F.-F. Jin, J. L. Conroy, The importance of ENSO nonlinearities in tropical pacific
1277 response to external forcing. *Clim. Dyn.* **49**, 2695–2704 (2017).
- 1278 73. A. C. Baker, D. F. Larcker, C. C. Y. Wang, How much should we trust staggered difference-in-
1279 differences estimates? *J. Financ. Econ.* **144**, 370–395 (2022).
- 1280 74. C. de Chaisemartin, X. D’Haultfoeuille, Two-Way Fixed Effects and Differences-in-Differences with
1281 Heterogeneous Treatment Effects: A Survey (2022), , doi:10.3386/w29691.

- 1282 75. J. Roth, P. H. C. Sant’Anna, A. Bilinski, J. Poe, What’s Trending in Difference-in-Differences? A
 1283 Synthesis of the Recent Econometrics Literature (2023), , doi:10.48550/arXiv.2201.01194.
- 1284 76. B. Callaway, P. H. C. Sant’Anna, Difference-in-Differences with multiple time periods. *J. Econom.*
 1285 **225**, 200–230 (2021).
- 1286 77. B. Callaway, A. Goodman-Bacon, P. H. C. Sant’Anna, Difference-in-Differences with a Continuous
 1287 Treatment (2021), , doi:10.48550/arXiv.2107.02637.
- 1288 78. C. de Chaisemartin, X. D’Haultfoeuille, Two-Way Fixed Effects Estimators with Heterogeneous
 1289 Treatment Effects. *Am. Econ. Rev.* **110**, 2964–2996 (2020).
- 1290 79. C. de Chaisemartin, X. D’Haultfoeuille, F. Pasquier, G. Vazquez-Bare, Difference-in-Differences
 1291 Estimators for Treatments Continuously Distributed at Every Period (2022), ,
 1292 doi:10.48550/arXiv.2201.06898.
- 1293 80. P. Jakiela, Simple Diagnostics for Two-Way Fixed Effects (2021), , doi:10.48550/arXiv.2103.13229.
- 1294 81. R. Knutti, J. Sedláček, B. M. Sanderson, R. Lorenz, E. M. Fischer, V. Eyring, A climate model
 1295 projection weighting scheme accounting for performance and interdependence. *Geophys. Res. Lett.*
 1296 **44**, 1909–1918 (2017).
- 1297 82. R. Knutti, The end of model democracy? *Clim. Change.* **102**, 395–404 (2010).
- 1298 83. P. Huang, J. Ying, A Multimodel Ensemble Pattern Regression Method to Correct the Tropical
 1299 Pacific SST Change Patterns under Global Warming. *J. Clim.* **28**, 4706–4723 (2015).
- 1300 84. D. Chen, M. A. Cane, S. E. Zebiak, R. Cañizares, A. Kaplan, Bias correction of an ocean-atmosphere
 1301 coupled model. *Geophys. Res. Lett.* **27**, 2585–2588 (2000).

1302

1303 **Supplementary Materials**

1304 Materials and Methods

1305 Supplementary Text

1306 References (49-84)

1307 Figs. S1 to S17

1308 Tables S1 to S7

1309

1310 **Acknowledgements.** We thank Dartmouth’s Research Computing and the Discovery Cluster for
 1311 computing resources. We thank the World Climate Research Programme, which, through its Working
 1312 Group on Coupled Modeling, coordinated and promoted CMIP6. **Funding:** This work was supported by
 1313 National Science Foundation Graduate Research Fellowship #1840344 to C.W.C. and grants from
 1314 Dartmouth’s Neukom Computational Institute, the Wright Center for the Study of Computation and Just
 1315 Communities, and the Nelson A. Rockefeller Center to J.S.M. **Author contributions:** Both authors

1316 designed the analysis. C.W.C. performed the analysis. Both authors interpreted the results and wrote the
1317 paper. **Competing interests:** The authors declare no competing interests. **Data and code availability:** All
1318 data and code that support of this study will be made available upon publication at
1319 github.com/ccallahan45/CallahanMankin_ENSOEconomics/.